nature biotechnology

Article

https://doi.org/10.1038/s41587-022-01524-7

# Time-tagged ticker tapes for intracellular recordings

Received: 13 October 2021

Accepted: 22 September 2022

Published online: 02 January 2023

Check for updates

Dingchang Lin[1,5,6] ✉, Xiuyuan Li[1,6], Eric Moult[1], Pojeong Park[1], Benjamin Tang[1], Hao Shen[2], Jonathan B. Grimm[3], Natalie Falco[3], Bill Z. Jia[1], David Baker[2], Luke D. Lavis[3] & Adam E. Cohen[1,4] ✉

Recording transcriptional histories of a cell would enable deeper understanding of cellular developmental trajectories and responses to external perturbations. Here we describe an engineered protein fiber that incorporates diverse fluorescent marks during its growth to store a ticker tape-like history. An embedded HaloTag reporter incorporates user-supplied dyes, leading to colored stripes that map the growth of each individual fiber to wall clock time. A co-expressed eGFP tag driven by a promoter of interest records a history of transcriptional activation. High-resolution multi-spectral imaging on fixed samples reads the cellular histories, and interpolation of eGFP marks relative to HaloTag timestamps provides accurate absolute timing. We demonstrate recordings of doxycycline-induced transcription in HEK cells and *cFos* promoter activation in cultured neurons, with a single-cell absolute accuracy of 30–40 minutes over a 12-hour recording. The protein-based ticker tape design we present here could be generalized to achieve massively parallel single-cell recordings of diverse physiological modalities.

A longstanding goal in biology is to map the dynamics of gene expression throughout a tissue or organism. Such maps could reveal mechanisms of spatial and temporal patterning, for example in brain activity, embryonic development or disease progression. Fluorescent protein-based markers are a powerful tool for mapping gene expression. However, optical imaging of fluorescent reporters faces a tradeoff between temporal and spatial information. Imaging in fixed tissue can report organ-wide patterns of gene expression but typically at only one[1,2] or, at most, two[3] timepoints. Time-lapse in vivo microscopy can report longitudinal gene expression dynamics[4] but only in a small optically accessible region, limited by light-scatter and optical instrumentation, and in vivo imaging typically requires surgery and/or immobilization of the animal. Theoretical analyses have explored the possibility of encoding organ-wide dynamics in DNA or RNA sequences[5,6], but, despite progress[7], such ideas have not yet been realized. Tools to record the dynamics of large numbers of cells, without constraints from in vivo imaging, could transform our ability to study ensemble dynamics in the nervous system and in other tissues.

Natural histories are written in the patterns of tooth enamel, the structures of pearls and the thickness of tree rings. The annual bands in tree rings mark the passage of time in a manner that is independent of variations in growth rate between trees or over years. These bands permit one to identify the timing of other events (for example, a forest fire) with absolute chronological accuracy. Inspired by these natural phenomena, we sought to encode cellular histories in protein microcrystals within individual cells. Protein assemblies can last for months or years and offer a wide array of functionalities, which could serve as the basis for recording schemes.

In this study, we developed a protein-based recording scheme that consists of three elements (Fig. 1a,b). First, a protein scaffold, which grows over time and which can incorporate fluorescent marks. Second, a means to impart fiducial timestamps to relate scaffold growth to the

[1]Department of Chemistry and Chemical Biology, Harvard University, Cambridge, MA, USA. [2]Institute for Protein Design, University of Washington, Seattle, WA, USA. [3]Janelia Research Campus, Howard Hughes Medical Institute, Ashburn, VA, USA. [4]Department of Physics, Harvard University, Cambridge, MA, USA. [5]Present address: Department of Materials Science and Engineering, Johns Hopkins University, Baltimore, USA. [6]These authors contributed equally: Dingchang Lin, Xiuyuan Li. ✉e-mail: dingchang@g.harvard.edu; cohen@chemistry.harvard.edu

timing of events in the outside world. By marking known timepoints on the fiber, one can correct for inevitable variations in fiber growth rate over time and between cells. Third, a fluorescent reporter of transcriptional activity, which can be stably incorporated into the scaffold. By measuring the position of the activity-driven marks relative to the fiducial timestamps, one can infer the timing of the transcriptional events with a precision substantially better than the timing between the timestamps and insensitive to cell-to-cell variations in growth rate. This procedure could enable recording of transcriptional activity with high absolute timing accuracy on a cell-by-cell basis.

For the protein scaffold, our selection criteria were that it should express in mammalian cells, assemble into a growing structure from a single polypeptide, have a known crystal structure, be unlikely to interfere with cellular physiology and accommodate decoration with a fluorescent tag without disrupting the structure of the assembly. We considered many possibilities, including endogenous microtubules, bacterial R-bodies[8], plant forisomes[9], amyloid fibrils[10], prions[11], filamentous viruses[12], crystals of the fluorescent protein XpA (ref. [13]), engineered fiber-forming peptides[14] and other proteins that spontaneously crystallize in cells[15].

A fusion of the catalytic domain of the Pak4 kinase and the 38 amino acid iBox domain of its inhibitor Inka1 (hereafter called iPAK4) largely satisfied the selection criteria. This construct has been shown to stably assemble in cells into rod-shaped crystals[16]. Remarkably, the crystal structure has a hexagonal array of internal pores large enough to accommodate eGFP or a HaloTag (HT), suggesting the possibility of linear encoding of information via patterned fluorescence (Fig. 1c).

We sought to use a fusion of the HT to iPAK4 to provide fiducial timestamps. We reasoned that washes with different colored HT ligand dyes could create color boundaries whose positions would correspond to known times. Even though HT dye washout in vivo occurs over hours, HT dye injection and labeling have fast onset (<10 minutes in vivo)[17], permitting precise demarcation of timestamps by the location of a color transition. A broad palette of bright, photostable and brain-penetrant Janelia Fluor (JF) HT ligand dyes are available, permitting diverse spectral encodings of fiducial timestamps[18–20].

The activity reporter should store a stable mark of cellular activity or physiology upon incorporation into the growing fiber. Here we focus on markers of transcriptional activation, although other modalities are conceivable. First, we mapped the kinetics of activation of a synthetic drug-inducible promoter, the Tet-ON system. Then, we mapped the dynamics of an activity-responsive immediate early gene (IEG) in cultured neurons. IEG reporters are a powerful tool for identifying the brain regions and neuronal subtypes activated in a particular context[21]. For example, the IEG *cFos* has been used to map neurons activated during feeding[22], sleep[23], parenting[24], aggression[25] and memory encoding[26]. IEG activation is a good target for a ticker tape recording because the relevant dynamics are often broadly distributed throughout the brain[26]. Motivated by potential applications toward brain-wide activity mapping, we used the *cFos* promoter to drive expression of eGFP-iPAK4 and, thereby, record time series of *cFos* activity.

## Results

### iPAK4 fibers grow linearly in HEK cells

In HEK cells co-transfected with CMV::iPAK4 (95%) and CMV::HT-iPAK4 (5%), fibers began to grow 14–20 hours after transfection. Incubation with an HT ligand dye made the fibers brightly fluorescent (Fig. 1d, Supplementary Fig. 1 and Methods). When the fibers grew longer than the cell diameter, the membrane deformed, forming a sheath around the fiber (Supplementary Fig. 1).

To assess the suitability of iPAK4 fibers as a recording medium, we performed a detailed characterization of their nucleation and growth. We co-expressed CMV::iPAK4 (90%), CMV::eGFP-iPAK4 (5%) and CMV::HT-iPAK4 (5%) in HEK cells using lentiviral transduction and added $JF_{669}$ to the medium to label the HT. We recorded time-lapse video microscopy over 43 hours, starting 20 hours after transfection (Methods and Supplementary Movie 1), and tracked the growth of individual fibers (Methods and Supplementary Movie 2). Initially, green (eGFP) and red (HT-$JF_{669}$) fluorescence accumulated in the cytoplasm. Upon nucleation, the fiber growth exhibited two clearly distinct phases. (1) Initially, fibers grew quickly (~0.5 μm $min^{-1}$) while the cytoplasmic fluorescence dropped. This phase typically lasted ~1 hour. (2) The fibers then transitioned to slower linear growth (Fig. 1e). Although there was substantial cell-to-cell variability in the rate of linear growth, the population-average growth rate did not change over 24 hours after nucleation (Fig. 1f). A simple mass action kinetic model predicted the two-phase growth profiles and quantitatively reproduced the observed growth profiles (Supplementary Calculation 1 and Supplementary Fig. 2).

We quantified the distribution of fiber growth parameters across the population. The length of fibers at the end of the nucleation phase was 26 ± 7 μm (mean ± s.d., $n = 46$ fibers; Fig. 1g). During the linear growth phase, the growth rate was 1.46 ± 0.64 μm $h^{-1}$ (mean ± s.d.; Fig. 1h). Within each cell, the fiber growth rate remained remarkably constant during the linear growth phase. During 24 hours, the fits of the growth profiles to straight lines yielded a population-average $R^2 = 0.97 \pm 0.02$ (mean ± s.d.; Fig. 1i). Of the cells that had any fibers, most contained only one (of 333 fiber-containing cells, 288 (86%) contained only one fiber). We ascribe the rarity of multiple fibers per cell to the fact that a single growing fiber maintained the soluble iPAK4 concentration below the nucleation threshold. Anecdotally, multi-fiber cells seemed to arise from cells where a fiber broke, leading to two nuclei.

Within the population, we observed cell-to-cell variations in the intensities of the eGFP and HT fluorescence signals, presumably due to variations in gene dosage. We did not observe any correlation between the growth rates and these fluorescence levels, indicating that, at the low mole fractions of fluorescent tags used here (approximately 5% for each fluorescent tag), the fluorescent tags did not affect the growth rate (Supplementary Fig. 3).

We then asked if the iPAK4 fibers affected cell survival, as the fibers often grew longer than the cell diameters (Supplementary Fig. 1). In a live/dead assay, we did not observe a difference in survival between HEK cells expressing iPAK4 fibers and control untransfected HEK cells ($iPAK4^+$: 0.267 ± 0.139% dead cells, $n = 24$ fields of view comprising 89,341 cells; $iPAK4^-$: 0.262 ± 0.107% dead cells, $n = 24$ fields of view comprising 94,202 cells; $P = 0.90$, Student's $t$-test; Supplementary Fig. 4). Alhough the stiff fibers deforming the cell membranes looked unusual, simple geometrical estimates showed that the fibers perturbed HEK cell surface area by <15% and volume by <2%, and the predicted fractional perturbations for neurons were even smaller (Supplementary Calculation 2).

We then tested whether cells containing iPAK4 fibers could divide. In taking time-lapse movies of HEK cells labeled with Hoechst 33342 nuclear stain, we observed occasional cell divisions. The formation of mitotic chromosomes and the process of cell division appeared qualitatively similar in cells with iPAK4 fibers, in cells expressing iPAK4 but without fibers and in non-expressing cells (Supplementary Fig. 5), although the number of mitotic events captured ($n = 8$ divisions in cells containing fibers) was too small for statistical analysis. Possible perturbations to cell division should be assessed separately in any cell type where iPAK4 fibers are used. We note that, for applications in neurons, cell division is not a concern. Together, these results established that iPAK4 fiber growth during the linear growth phase formed a suitable substrate for cellular recordings, provided one could correct for cell-to-cell variations in growth rate.

### HT timestamps enable accurate timing in iPAK4 fibers

To test whether fibers could encode HT dye timestamps, we successively washed HEK cells growing HT-iPAK4 fibers with different colors of

https://doi.org/10.1038/s41587-022-01524-7

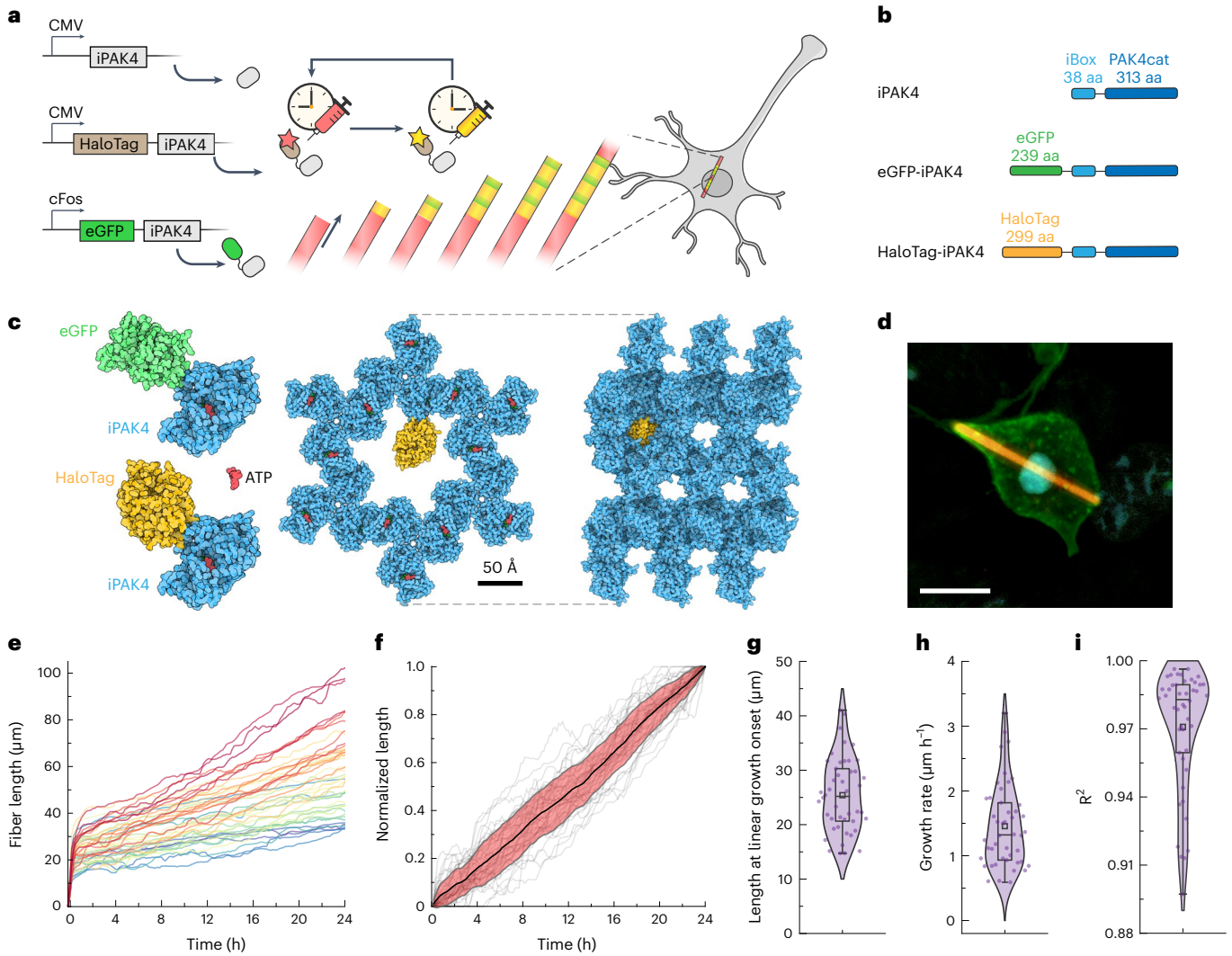


**Fig. 1 | iPAK4 forms intracellular protein fibers. a**, Scheme for intracellular recording of cFos activity with fiducial timestamps. iPAK4 forms the fiber scaffold. HaloTag-iPAK4 incorporates HT dyes, permitting labeling of the fiber with fiducial timestamps. Neural activation drives expression of cFos::eGFP-iPAK4, introducing green bands into the fiber. **b**, Composition of the protein constructs used to label intracellular protein fibers. **c**, The structures of tagged iPAK4 monomers and the crystal structure with hexagonal pores (from the Protein Data Bank: 4XBR) were modeled using Protein Imager software[35]. **d**, Image of a HEK cell expressing CMV::iPAK4 (95%) and CMV::HT-iPAK4 (5%). The fiber was stained with $JFX_{608}$; the membrane was labeled by expressing GPI-eGFP; and the nucleus was labeled with DAPI. Scale bar, 10 µm. **e**. Growth profiles of iPAK4 fibers in HEK cells ($n = 46$ fibers). **f**, Population average (black) and standard deviation (red) of the linear-phase fiber growth (gray lines). Here, each fiber's linear-phase growth profile was mapped to the interval [0, 1]. **g**–**i**, Statistics of fiber growth ($n = 46$ fibers), showing **g**, fiber length at the transition from initial nucleation to linear growth; **h**, linear-phase growth rate; and **i**, $R^2$ of the fit of the linear-phase growth to a straight line. In **e**–**i**, fibers were randomly selected from Supplementary Movie 1. Box bounds: 25th and 75th percentile; whiskers: minimum and maximum; squares: mean; and center lines: median. All data points are displayed. aa, amino acid.

HT ligand dyes at $\Delta t = 2$-hour intervals in the sequence $JF_{503}$, $JF_{669}$, $JFX_{608}$, $JF_{503}$ and $JF_{669}$ (Fig. 2a; see Supplementary Fig. 6 for dye structures, photophysical properties and synthesis of $JFX_{608}$). We then fixed the cells and imaged them with spectrally resolved confocal microscopy (Methods). We observed clear progression of colored bands matching the sequence of dye additions. The bands followed mirror-image patterns on opposite sides of the fibers, indicating that the fibers grew from both ends (Fig. 2b and Supplementary Fig. 7).

To test the limits of how fast we could encode dye transitions, we made fibers with seven dye switches at $\Delta t = 1$ hour. Although peaks were still visible at this short interval, their amplitude was suppressed relative to the parts of the fiber with no dye switches, indicating incomplete transitions in dye labeling (Supplementary Fig. 7e). Analysis of the dye profiles for more widely spaced dye transitions indicated a half-life of soluble HT-iPAK4 of 4.5 hours (Supplementary Fig. 8a), explaining the loss of signal at faster dye switches. These results indicated that fiducial timestamps should be separated by at least $\Delta t = 2$ hours.

Dye additions appeared as upward-going kinks in the fluorescence profiles (Supplementary Fig. 8a), which we located as peaks in the second derivative of fluorescence version position (Methods). By dividing the transition zone widths (full-width at half-maximum of the peak in the second derivative) by the fiber-specific growth rates, we calculated a mean transition zone duration of 7.5 minutes (Supplementary Fig. 8a).

To determine the influence of HT dye labeling kinetics on the widths of these transitions, we measured the labeling of intracellular HT receptors with different HT dyes (Methods). These measurements probed the combined effects of membrane permeation and the HT reaction. The effective time constants at 1 µM dye were: 43 minutes ($JF_{503}$), 3.5 minutes ($JF_{525}$), 2.0 minutes ($JF_{552}$), 12 minutes ($JFX_{608}$) and 17 minutes ($JF_{669}$) (Supplementary Fig. 8). The precision of localizing

https://doi.org/10.1038/s41587-022-01524-7

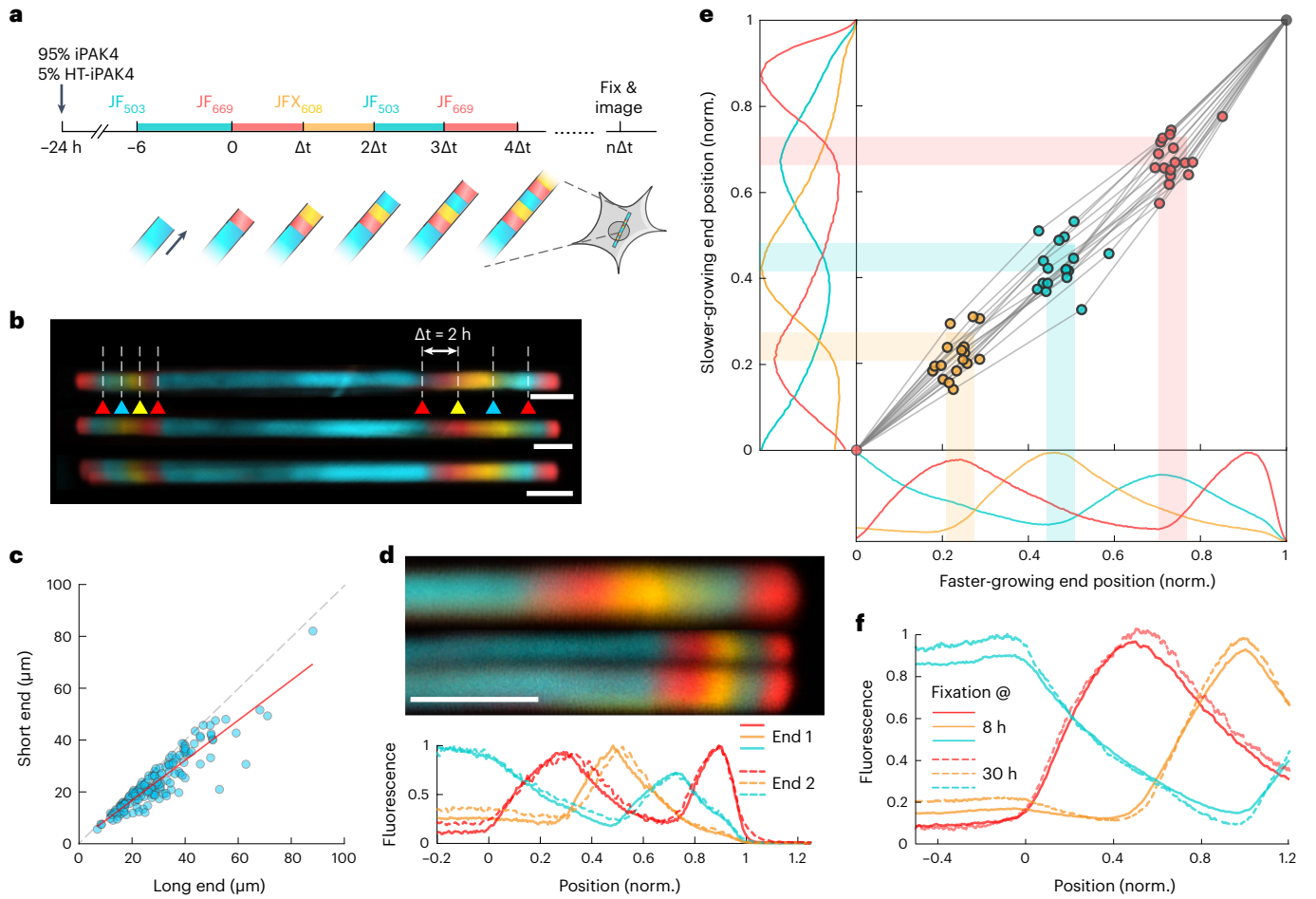


**Fig. 2 | iPAK4 fibers can be sequentially labeled with different dyes. a**, Scheme for multi-color labeling of intracellular iPAK4 fibers. **b**, Images of iPAK4 fibers labeled with four dye transitions on each end. Triangles indicate times of dye addition. Cyan: $JF_{503}$, Red: $JF_{669}$, Yellow: $JFX_{608}$. Scale bars, 5 μm. **c**, Comparison of the growth rate on the two ends after one dye switch. The long end and short end correspond to the faster-growing end and slower-growing end, respectively ($n = 153$ fibers). The growth rate on the slower-growing end was 0.77 ± 0.05 of that on the faster-growing end (95% CI). **d**, Comparison of two ends of a single fiber. Top: images of the two ends. In this case, the fiber split at one of its ends, an occurrence in approximately 10% of fibers. Bottom: quantification of the fluorescence traces in the two ends, with position normalized to the locations of the first $JF_{669}$ addition and the end of the fiber. Scale bar, 5 μm. **e**, Comparison of dye transition points on the faster-growing and slower-growing fiber ends. The scatter plot shows the positions of the $JFX_{608}$, $JF_{503}$ and $JF_{669}$ transitions normalized relative to the first $JF_{669}$ addition (at position 0) and the end of the fiber (at position 1). The plots show the mean fluorescence profiles of $n = 17$ fibers. Here, the number of fibers was set by the requirement for in-focus, unobstructed views of both ends of the fibers. **f**, Mean fluorescence profiles of fibers exposed to the same sequence of dyes and then grown for different amounts of time ($n = 22$ fixed at 8 hours, 12 fixed at 30 hours). The overlap of these profiles indicates negligible monomer exchange over 22 hours.

a dye transition in a fiber is not equal to the labeling time constant but, rather, the precision with which one can identify the onset of the labeling reaction. For all the JF dyes, this time was much less than 10 minutes. Together, these results established that HT dye transitions provided a means to timestamp iPAK4 fiber growth with a local precision (that is, around the time of a timestamp) of ~10 minutes or better.

Due to the $P6_3$ symmetry of the iPAK4 crystal structure[16], the two ends are not chemically equivalent and need not have the same growth rate. However, the asymmetry in growth rate was modest: the growth rate on the slower-growing end was 0.77 ± 0.05 (95% confidence interval (CI)) of the growth rate on the faster-growing end (Fig. 2c). We then compared the fluorescence profiles on the two ends. To account for the difference in growth rate between the fiber ends, we mapped the first dye addition ($JF_{669}$ at $t = 0$) to $x = 0$ and the end of the fiber (fixation at $t = 8$ hours) to $x = 1$. After normalizing the spatial scales, the fast-growing and slow-growing fiber ends showed very similar profiles (Fig. 2d).

To test whether both fiber ends could be useful for recording fiducial timestamps, we analyzed the locations of the dye transitions on both ends of $n = 17$ fibers. For both the faster-growing and slower-growing ends, the normalized locations of dye transitions at $t = 2$, 4 and 6 hours mapped linearly onto position between the first dye addition ($t = 0$) and the end of the fiber ($t = 8$ hours) (Fig. 2e). The standard deviations in the inferred timing (averaging over the three transitions) were 18.3 minutes on the fast end and 24.8 minutes on the slow end. Together, these results established that both ends of the fibers could record fiducial timestamps with an absolute accuracy of better than 25 minutes over an 8-hour baseline.

If the residual errors in timing were driven by a factor shared by the two fiber ends (for example, variations in iPAK4 expression level), then these errors would lie primarily along the diagonal line Position 1 = Position 2 in Fig. 2e. We calculated the cross-correlation in the timing errors between the two fiber ends and averaged over all transitions ($t = 2$, 4 and 6 hours) and all fibers. This cross-correlation was only 0.32, implying that dynamic fluctuations in growth rate were primarily

driven by factors local to each end. In principle, timing precision could be improved by averaging measurements on the two fiber ends, but we found that, often, the image quality was better on one end than the other because of differences in the focal plane or the presence of out-of-focus fibers. Consequently, we typically analyzed only one fiber end per cell, and we did not attempt to distinguish between the faster-growing and slower-growing ends.

A protein ticker tape should stably store its information for extended times. Because the iPAK4 fibers were held together by non-covalent interactions, we tested whether monomer exchange blurred the HT dye boundaries over time. Two dishes were exposed to the same sequence of dye switches at intervals of $\Delta t = 2$ hours. One dish was fixed at $t = 8$ hours, and the other was returned to the incubator and fixed 1 day later at $t = 30$ hours. We then compared the fluorescence profiles for the section of the fibers that grew concurrently (from $t = 0$ to 8 hours). The mean profiles were nearly indistinguishable between the early dish ($n = 22$ fibers) and the late dish ($n = 12$ fibers) (Fig. 2f). Thus, monomer exchange was negligible over 1 day.

We next studied the precision with which the timing of cellular events could be identified. If each fiber end grew at a constant rate, the timing of cellular events could be linearly interpolated between timestamps with a precision far greater than the interval between the timestamps. However, fluctuations in the growth rate might degrade the precision. To determine the precision empirically, we incubated fibers in $JF_{525}$ and then switched to $JF_{669}$ at $t = 0$. In different dishes, we doped in the dye $JFX_{608}$ at $t = 2$, 4, 6, 7, 8 or 9 hours to simulate the onset of a cellular event. Finally, we switched back to $JF_{525}$ at $t = 10$ hours, grew the fibers for another 10 hours and fixed the dishes at $t = 20$ hours (Fig. 3a). Low-magnification images showed clear stripes in most fibers, corresponding to the timestamps and the addition of $JFX_{608}$ (Fig. 3b).

Visual inspection of the fibers with $JFX_{608}$ addition at different timepoints showed clear onset of yellow staining at the corresponding positions along the red band (Fig. 3c). We quantified the three-color fluorescence profiles of $n = 223$ fibers (20–51 fibers per timepoint of $JFX_{608}$ addition) and identified the locations of the three dye additions ($JF_{669}$, $JFX_{608}$ and $JF_{525}$). As above, we mapped each fluorescence trace so that the first and third dye additions occurred at $x = 0$ and 1, respectively (Fig. 3d).

The mean traces clearly showed the time-dependent onset of $JFX_{608}$ fluorescence, which was also evident in low-magnification images of the fiber population (Supplementary Fig. 9). We then quantified the distributions of $JFX_{608}$ onset. The distribution linearly mapped dye addition time to normalized position between 0 and 1 (Fig. 3e). Mapping the standard deviation of $JFX_{608}$ labeling onset onto the 10-hour time axis yielded single-fiber precisions between 25 and 51 minutes (Fig. 3e). The precision was greatest near the fiducial points at $t = 0$ and 10 hours and lowest in the middle of the trajectory. This observation established that the uncertainty in $JFX_{608}$ timing was dominated by intracellular fluctuations in the fiber growth rate, as opposed to errors in locating the $JFX_{608}$ transition points, because localization errors would be statistically similar anywhere along the fiber. Thus, to achieve the greatest temporal precision for detecting an event, one should deposit a fiducial timestamp near the candidate event.

## Time-tagged iPAK4 fibers record dynamics of gene expression

As the first test of a physiological recording, we used iPAK4 fibers to report on a transcriptional activator, the tetracycline-mediated Tet-ON transcription system[27]. We co-infected HEK cells with lentivirus containing CMV::iPAK4 (60%), CMV::rTTA3 (30%), CMV::HT-iPAK4 (5%) and TRE::eGFP-iPAK4 (5%) to establish tetracycline-dependent eGFP-iPAK4 expression (Fig. 4a). After fibers had nucleated (24 hours after lentiviral infection), we added $JF_{552}$ to label the initial nuclei and then switched to $JF_{669}$ at $t = 0$. In different dishes, we added doxycycline (DOX, 2 μg ml$^{-1}$) at $t = 2$, 4 or 6 hours to activate expression of eGFP-iPAK4. Then, we switched back to $JF_{552}$ at $t = 8$ hours and grew the fibers for another 8–14 hours before fixation and imaging (Fig. 4b).

DOX addition led to formation of green bands in the fibers, with onset at positions linearly related to DOX addition time ($n = 191$ fibers; Fig. 4c,d). Based on the fiber-to-fiber variations in the positions of the green onsets, we inferred an absolute timing accuracy of 30–40 minutes over an 8-hour baseline. A linear fit to the band positions yielded an apparent offset of 1.2 hours between DOX addition and the start of the green stripe. We ascribe this delay to the time required for transcription, translation and protein folding. Similar experiments where cells were exposed to a 30-minute pulse of DOX caused eGFP-iPAK4 expression to rise for approximately 8 hours and then fall, leading to a ~14-hour window of protein expression (Supplementary Fig. 10). These experiments demonstrate that the iPAK4 ticker tape system can quantify the dynamics of promoter activity in single cells.

The Tet-ON system also provides a means to control the onset of iPAK4 nucleation, allowing a separation between gene delivery and the start of a recording. We co-expressed CMV::rtTA3 (30%), TRE::iPAK4 (65%) and TRE::eGFP-iPAK4 (5%) in HEK cells using lentiviral transduction and added DOX after 7 days (Supplementary Fig. 11). In the first 7 days, we observed negligible eGFP signal, indicating minimal background expression of the Tet-ON system. After DOX addition, iPAK4 fibers were observed starting on day 8, with clear elongation of the fibers over the following day. Inducible ticker tape expression could be a powerful tool for defining recording windows to coincide with specific experimental perturbations.

## Time-tagged iPAK4 fibers record neural activation

Finally, we tested the ability of iPAK4 ticker tapes to report activation of the IEG *cFos* promoter in cultured rat hippocampal neurons. To establish iPAK4 fiber recordings in neurons, we first verified that (1) the fibers grew linearly in neurons; (2) a dye switch introduced fiducial timestamps in neurons; and (3) the fibers did not introduce cytotoxicity or changes to neuronal electrophysiology.

To characterize fiber growth in neurons, we performed time-lapse imaging over 33 hours in a primary neuron culture lentivirally infected with CMV::iPAK4 (90%) and CMV::HT-iPAK4 (10%) (Supplementary Movie 4). Fibers of iPAK4 nucleated and grew in neurons following a similar trajectory to in HEK cells, comprising a fast-growing nucleation phase followed by slower linear growth (Supplementary Fig. 12 and Supplementary Movie 5). We occasionally observed fibers stall for a few hours or sometimes stop growing altogether. Stalled fibers were flagged by requiring a mean growth rate of >0.8 μm h$^{-1}$. This excluded 11 of 33 tracked fibers (33%). A key point is that the growth rate threshold could be applied based on a single terminal measurement of fiber length and, thus, did not require time-lapse imaging.

Of the fibers that passed the growth rate criterion, the fiber length at onset of linear growth was 31 ± 12 μm (mean ± s.d., $n = 22$ fibers). The growth rate in the linear phase was 2.5 ± 1.5 μm h$^{-1}$. During the linear growth phase, the fit to a straight-line growth profile had a mean $R^2 = 0.95 \pm 0.04$, over a 24-hour interval. Of the neurons that had fibers, most (73%) had only one fiber, although many neurons did not have fibers nucleated at the time of the recording (Supplementary Fig. 13). We also performed dye switch experiments in neurons and confirmed the ability of switches in HT dye labeling to impart fiducial timestamps on HT-iPAK4 fibers in neurons (Supplementary Figs. 14 and 15).

To test for effects of iPAK4 fibers on neuronal survival, we lentivirally expressed iPAK4 (95%) and HT-iPAK4 (5%) in cultured neurons, allowed the fibers to grow for 6 days and then performed a live/dead assay (Supplementary Fig. 16). There was no significant difference in the fraction of dead cells between dishes expressing iPAK4 fibers and dishes not infected with any lentivirus. The iPAK4-expressing neurons had typical soma and neurite structures, similar to those observed in healthy neurons.

https://doi.org/10.1038/s41587-022-01524-7

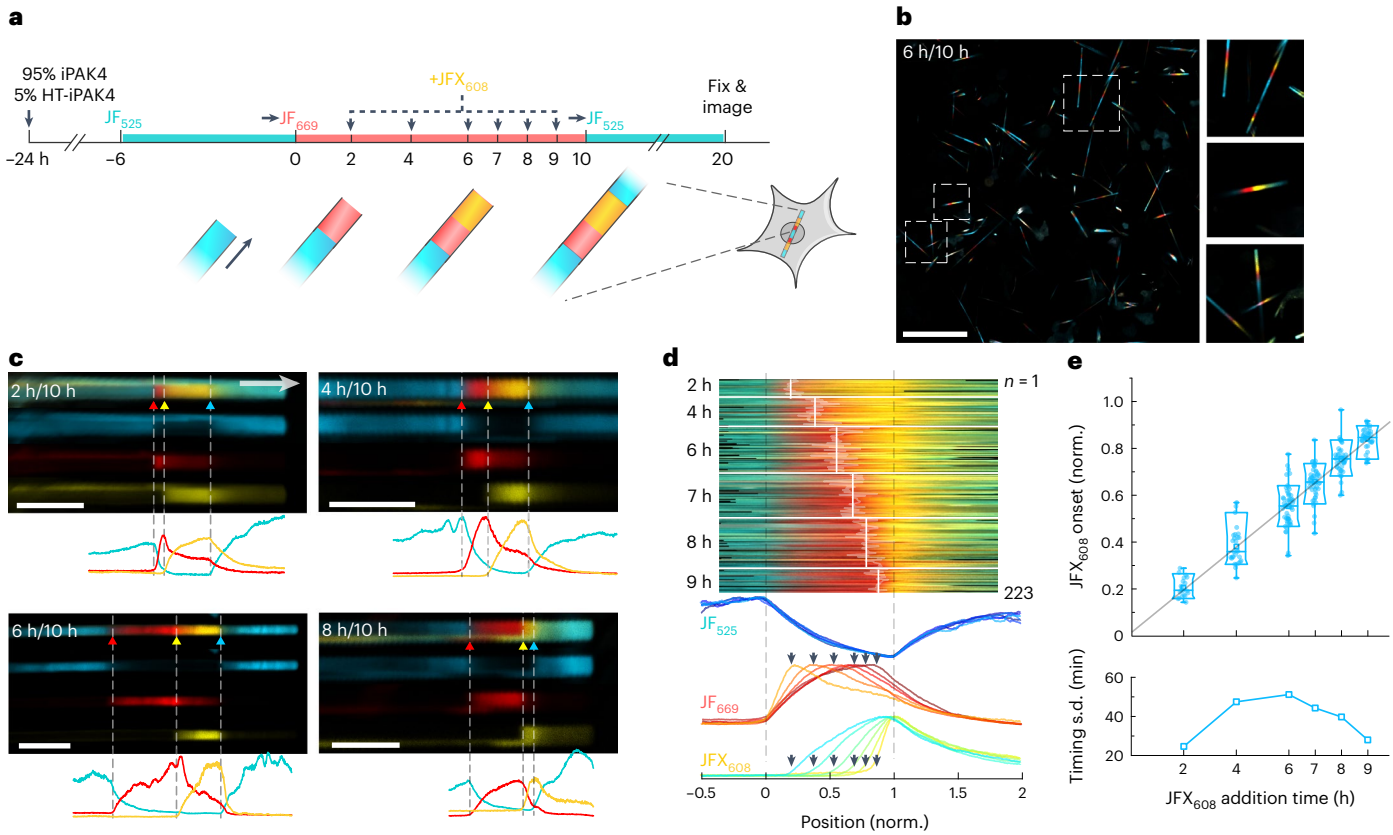


**Fig. 3 | iPAK4 fibers report timing of intracellular events. a**, Experimental design for testing the precision with which addition of $JFX_{608}$ could be determined relative to timestamps from addition of $JF_{669}$ (at $t = 0$) and $JF_{525}$ (at $t = 10$ hours). **b**, Low-magnification (left) and magnified (right) images of iPAK4 fibers in HEK cells. Scale bar, 100 µm. **c**, Top: images of fibers with $JFX_{608}$ addition at $t = 2$, 4, 6 and 8 hours. Bottom: fluorescence line profiles. Scale bars, 10 µm. **d**, Top: fluorescence profiles of $n = 223$ fiber ends with $JFX_{608}$ addition at different timepoints. The profile lengths have been normalized to line up the timestamps at $t = 0$ and 10 hours. Bottom: mean fluorescence traces in each of the three dye color channels, for all times of $JFX_{608}$ addition. **e**, Top: positions of the $JFX_{608}$ onset as a function of dye addition time. Bottom: standard deviation in the inferred timing of $JFX_{608}$ addition for each population of fibers ($n = 223$ fiber ends). Lower and upper bounds of the box plot: 10th and 90th percentiles; lower and upper whiskers: minimum and maximum; squares: mean; and center lines: median. All data points are displayed.

We then tested whether iPAK4 fibers affected neuronal electrophysiology. Neurons infected with lentivirus containing payloads CMV::iPAK4 (90%) and CMV::eGFP-iPAK4 (10%) grew single straight fibers (Fig. 5a). We used patch-clamp recordings to compare the electrophysiology of neurons with and without fibers. Although, in many cases, the fiber length was several times longer than the soma diameter, neurons with fibers spiked normally (Fig. 5b) and had membrane resistance, membrane capacitance, resting potential and rheobase, which were statistically indistinguishable from neurons without fibers ($n = 11$ neurons with fibers and $n = 12$ neurons without, two-sided Student's $t$-test; Fig. 5c).

In neurons co-expressing CMV::iPAK4 (90%) and cFos::eGFP-iPAK4 (10%), fibers initially grew with little green fluorescence. Addition of phorbol 12-myristate 13-acetate (PMA, 1 µM), an activator of cFos expression[28], led to bands of bright green fluorescence (Supplementary Fig. 8). Sequential additions of PMA to a single dish led to distinct bands of eGFP fluorescence, clearly resolved by sharp eGFP boundaries (Fig. 5d).

To measure timing of cFos activation relative to fiducial timestamps, we co-expressed CMV::iPAK4 (80%), CMV::HT-iPAK4 (10%), and cFos::eGFP-iPAK4 (10%) (Fig. 5e). We stained the neurons with $JF_{552}$ and then switched to $JF_{669}$ at $t = 0$. We then added PMA (1 µM) at $t = 3$, 6 or 9 hours and introduced a second fiducial timestamp by switching back to $JF_{552}$ at $t = 12$ hours. Fibers were grown until $t = 22$ hours and then fixed and imaged (Fig. 5f).

We observed clear green bands, indicating cFos-driven expression of eGFP-iPAK4. To infer an onset time for each band, we mapped the onset of eGFP fluorescence relative to the two dye switches. The slope of the plot of inferred eGFP onset time versus nominal PMA addition time was 0.98 ± 0.10 (mean ± 95% CI, $n = 34$ fibers at 3 hours, 32 fibers at 6 hours and 40 fibers at 9 hours). Extrapolating this fit to $t = 0$ implied that eGFP onset was delayed by 53 minutes relative to the timing of PMA addition (Fig. 5h). We interpret this delay as the time for PMA to activate the cFos promoter plus delays of transcription, translation and protein folding of eGFP-iPAK4. The standard deviations in the inferred eGFP onset times were 34 minutes (3 hours), 50 minutes (6 hours) and 34 minutes (9 hours), implying an average absolute timing accuracy of 39 minutes over a measurement with 12 hours between fiducial timestamps.

## Discussion

Slowly growing protein assemblies are a promising substrate for massively parallel cellular recordings. Our recording strategy relies on three key elements: a protein scaffold, a means to impart fiducial timestamps and a fluorescent reporter of cellular activity, which is irreversibly incorporated into the scaffold during growth. Here, we validated the system with externally applied perturbations (drug-induced gene expression), which led to synchronous population-wide responses; but, in principle, the system is also capable of recording spontaneous or asynchronous activation of reporter genes.

https://doi.org/10.1038/s41587-022-01524-7

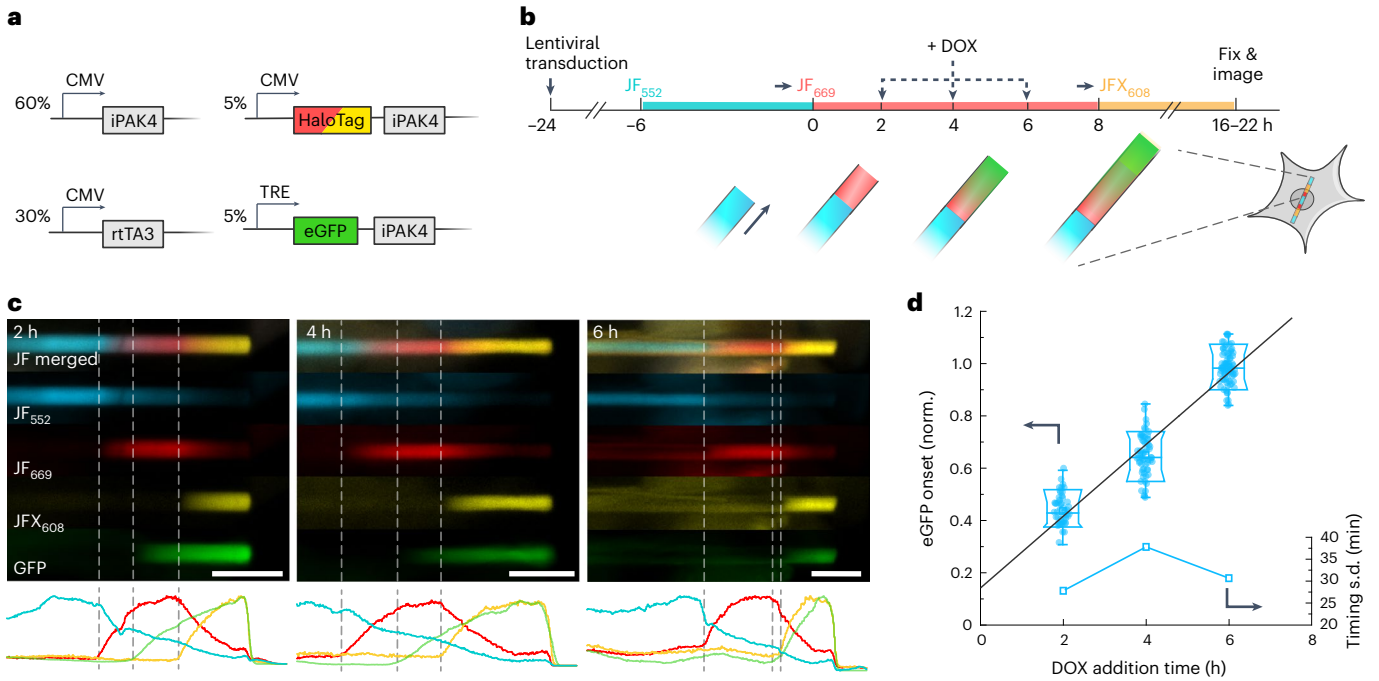


**Fig. 4 | Protein ticker tape recordings of DOX activation of the Tet-ON system in HEK cells. a**, Genetic constructs for recording time-tagged transcription activation. **b**, Experimental protocol for recording time-tagged transcription activation. Transitions to $JF_{669}$ at $t = 0$ and to $JFX_{608}$ at $t = 8$ hours provided fiducial timestamps. Transcription was activated via addition of DOX at $t = 2$, 4 or 6 hours. **c**, Top: representative images of fibers with DOX addition at $t = 2$, 4 or 6 hours. Bottom: fluorescence line profiles. Scale bars, 10 µm. **d**, Normalized positions of eGFP onset relative to fiducial timestamps at $t = 0$ and 8 hours. The linear fit has a $y$-intercept of 1.2 hours, indicative of the delay between DOX addition and protein synthesis ($n = 191$ fibers). Lower and upper bounds of the box plot: 10th and 90th percentiles; lower and upper whiskers: minimum and maximum; squares: mean; and center lines: median. All data points are displayed.

The fiducial timestamps are a particularly important conceptual and practical aspect of our approach. Timestamps permit detection, and in some cases correction, of many sources of variability that could otherwise confound the recordings. Here, we used the timestamps to correct for cell-to-cell variations in the linear-phase growth rate via a simple linear interpolation scheme. The timestamps could also flag individual cells in which there were substantial fluctuations in growth rate during a recording. These would manifest as distinct stripes having widths out of proportion to the corresponding dye incubation times. The timestamps could also flag fibers that nucleated after the first dye switch: such fibers would have their central portion tagged with a mixture of dyes instead of solely with the first dye. Fibers that fractured or aggregated would have timestamps that deviated from the anticipated color order. Thus, the timestamps provide a robust means of calibration and quality control within each cell.

There are opportunities to broaden and improve upon our approach regarding each of the three key elements: the scaffold, the timestamps and the physiological signal. For applications in vivo, the most critical need is to modify the scaffold so that it does not deform the cells. One approach is to engineer thinner fibers, either by modifying the iPAK4 scaffold to enhance the ratio of axial to radial growth or by using a different fiber-forming protein scaffold[14]. Thinner fibers would undergo Euler buckling at the cell membrane rather than deforming the cell, although, if the fiber becomes so thin that the thermal persistence length is smaller than a few microns, optical tracking of the fiber backbone could be difficult. Alternatively, one could explore alternate ticker tape geometries, such as helical aggregates (thereby achieving a ratio of contour length to axial length that exceeds 1) or spherical onion-type aggregates.

A second improvement to the scaffolds would be to decrease the ratio between the soluble iPAK4 concentration at fiber nucleation, $C_{nuc}$, and the concentration during steady-state growth, $C_{SS}$. Fits to the simple kinetic model of fiber growth (Supplementary Fig. 2) suggest that this ratio is currently ~100. Consequences of this high ratio are that (1) there is a highly variable delay of approximately 12 hours between onset of iPAK4 transcription and fiber nucleation, and (2) the fibers undergo a period of fast and non-linear growth during the first ~hour after nucleation (Fig. 1e). On the other hand, to ensure that most cells contain only a single fiber, one wants $C_{nuc}/C_{SS} > 1$. Thus, a protein engineering goal is to make this ratio slightly larger than 1.

Cultured neurons could sustain iPAK4 fiber growth for at least 6 days (Supplementary Fig. 16), suggesting the possibility of multi-day recordings. To tune the dynamic range of ticker tape recordings, one would like small-molecule or light-induced control over the onset and rate of ticker tape scaffold growth. Putting the iPAK4 scaffold under control of the Tet-ON system gave control over the onset of fiber growth (Supplementary Fig. 11). However, the slow transcriptional response to changes in DOX concentration (Supplementary Fig. 10), together with the high ratio of $C_{nuc}/C_{SS}$, meant that subsequent tuning of the growth rate by DOX concentration was not feasible by this approach. Achieving control over the rate of fiber growth would require either lowering $C_{nuc}/C_{SS}$ or developing alternate means of regulating protein assembly into the fiber, for example by pharmacological or optical regulation of protein stability[29] or of protein–protein interactions. Finally, one may want to express both the iPAK4 and the HT-iPAK4 from a single vector, either by making use of endogenous RNA splicing machinery or by applying a partially effective self-cleaving peptide.

At present, the spacing of the fiducial timestamps is constrained to ~2 hours by the ~4.5-hour half-life of soluble HT-iPAK4. If one could shorten this half-life, one could place timestamps closer together and, thereby, achieve greater absolute timing accuracy. One might shorten the half-life of the soluble HT-iPAK4 by attaching ubiquitination domains or other tags to facilitate proteolytic turnover of the soluble subunits[30]. Alternatively, one might consider a variety of optogenetic

https://doi.org/10.1038/s41587-022-01524-7

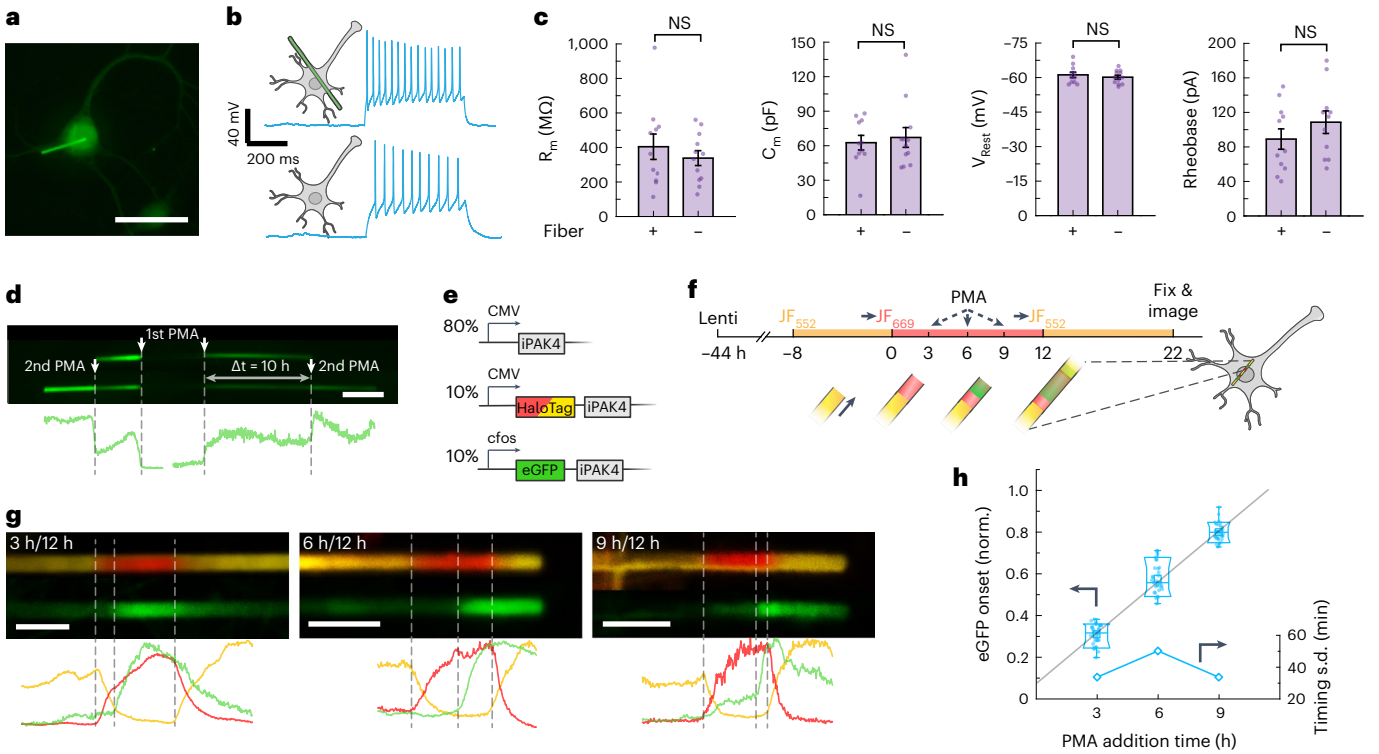


**Fig. 5 | Protein ticker tape recordings of cFos activation in neurons. a**, Image of a cultured neuron expressing lentiviral CMV::iPAK4 (90%) and CMV::eGFP-iPAK4 (10%). Scale bar, 50 µm. **b**, Representative patch-clamp recordings in neurons with or without an iPAK4 fiber. Spikes were evoked by a current injection of 100 pA. **c**, There were no significant differences between neurons with or without fibers in membrane resistance (404 ± 73 MΩ versus 339 ± 43 MΩ, $P = 0.43$), membrane capacitance (63 ± 6 pF versus 67 ± 9 pF, $P = 0.67$), resting potential (−61.2 ± 1.2 mV versus −60.2 ± 0.8 mV, $P = 0.48$) or rheobase (89 ± 12 pA versus 109 ± 13 pA, $P = 0.27$) ($n = 11$ neurons with fibers, 12 neurons without). Error bars show mean ± s.e.m. Two-sided Student's $t$-test was employed for data comparison. **d**, Fiber in a neuron expressing lentiviral CMV::iPAK4 (90%) and cFos::eGFP-iPAK4 (10%). The top image shows the fiber after a first PMA addition; the bottom image shows the same fiber after a second PMA addition. Scale bar, 5 µm. **e**, Genetic constructs for recording time-tagged cFos activation in neurons. **f**, Experimental protocol for recording time-tagged cFos activation in neurons. Transitions to $JF_{669}$ at $t = 0$ and to $JF_{552}$ at $t = 12$ hours provided fiducial timestamps. cFos was activated by addition of PMA at $t = 3$, 6 or 9 hours. **g**, Top: representative images of fibers with PMA addition at $t = 3$, 6 or 9 hours. Bottom: fluorescence line profiles. Scale bars, 5 µm. **h**, Normalized positions of eGFP onset relative to fiducial timestamps at $t = 0$ and 12 hours ($n = 106$ fibers). Lower and upper bounds of the box plot: 10th and 90th percentiles, respectively; lower and upper whiskers: minimum and maximum, respectively; squares: mean; and center lines: median. The linear fit has a $y$-intercept of approximtely 1.0 hour. All data points are displayed. NS, not significant.

caging strategies to reversibly control the availability of timestamp monomers[31]. Optogenetic modulation of protein availability can occur over seconds, suggesting the possibility to introduce extremely precise fiducial timestamps.

Finally, the modular design of iPAK4 fibers could be adapted to accommodate diverse recording modalities. A simple generalization of the present results would be to record the simultaneous dynamics of multiple promoters by using each to drive expression of iPAK4 fused to a spectrally distinct fluorescent protein. There also exist diverse fluorescent reporters of covalent enzymatic modifications, for example of kinase, phosphatase or protease activity[32,33]. Such reporters are likely protected from enzymatic modification within the fiber and, thereby, might be a means to record the state of the cell at the moment of incorporation into the fiber.

A related protein-based recording technique was introduced concurrent with our work, termed expression recording islands (XRIs)[34]. The primary conceptual difference between the XRIs and our time-tagged ticker tapes is that our HT-based timestamps give our ticker tapes an absolute time base in each single cell.

Despite the broad scope for improvements on the existing ticker tape system, we think that these tools are already suitable for applications in vitro. For instance, they could be used to map transcriptional dynamics during stem cell differentiation, in in vitro tumor models or in diverse organoid models. In each new cellular preparation, it will be critical to test whether expression of iPAK4 fibers perturbs the physiological dynamics of interest. The introduction of protein-based ticker tapes in our work and the XRIs in the companion paper[34] should spur diverse efforts on improving and applying these tools.

## Online content

Any methods, additional references, Nature Research reporting summaries, source data, extended data, supplementary information, acknowledgements, peer review information; details of author contributions and competing interests; and statements of data and code availability are available at https://doi.org/10.1038/s41587-022-01524-7.

## References

1. Renier, N. et al. Mapping of brain activity by automated volume analysis of immediate early genes. *Cell* **165**, 1789–1802 (2016).
2. Vetere, G. et al. Chemogenetic interrogation of a brain-wide fear memory network in mice. *Neuron* **94**, 363–374.e4 (2017).
3. DeNardo, L. A. et al. Temporal evolution of cortical ensembles promoting remote memory retrieval. *Nat. Neurosci.* **22**, 460–469 (2019).
4. Mahringer, D. et al. Expression of c-Fos and Arc in hippocampal region CA1 marks neurons that exhibit learning-related activity changes. Preprint at *bioRxiv* https://doi.org/10.1101/644526 (2019).

5. Zamft, B. M. et al. Measuring cation dependent DNA polymerase fidelity landscapes by deep sequencing. *PLoS ONE* **7**, e43876 (2012).
6. Glaser, J. I. et al. Statistical analysis of molecular signal recording. *PLoS Comput. Biol.* **9**, e1003145 (2013).
7. Rodriques, S. G. et al. RNA timestamps identify the age of single molecules in RNA sequencing. *Nat. Biotechnol.* **39**, 320–325 (2021).
8. Pond, F. R., Gibson, I., Lalucat, J. & Quackenbush, R. L. R-body-producing bacteria. *Microbiol. Mol. Biol. Rev.* **53**, 25–67 (1989).
9. Pélissier, H. C., Peters, W. S., Collier, R., Bel, A. J. Evan & Knoblauch, M. GFP tagging of sieve element occlusion (SEO) proteins results in green fluorescent forisomes. *Plant Cell Physiol.* **49**, 1699–1710 (2008).
10. LeVine, H. III. Quantification of β-sheet amyloid fibril structures with thioflavin T. *Methods Enzymol.* **309**, 274–284 (1999).
11. Barmada, S. J. & Harris, D. A. Visualization of prion infection in transgenic mice expressing green fluorescent protein-tagged prion protein. *J. Neurosci.* **25**, 5824–5832 (2005).
12. Shukla, S. et al. Molecular farming of fluorescent virus-based nanoparticles for optical imaging in plants, human cells and mouse models. *Biomater. Sci.* **2**, 784–797 (2014).
13. Tsutsui, H. et al. A diffraction-quality protein crystal processed as an autophagic cargo. *Mol. Cell* **58**, 186–193 (2015).
14. Shen, H. et al. De novo design of self-assembling helical protein filaments. *Science* **362**, 705–709 (2018).
15. Nguyen, T. K. et al. In-cell engineering of protein crystals with nanoporous structures for promoting cascade reactions. *ACS Appl. Nano Mater.* **4**, 1672–1681 (2021).
16. Baskaran, Y. et al. An in cellulo-derived structure of PAK4 in complex with its inhibitor Inka1. *Nat. Commun.* **6**, 8681 (2015).
17. Abdelfattah, A. S. et al. Bright and photostable chemigenetic indicators for extended in vivo voltage imaging. *Science* **365**, 699 (2019).
18. Grimm, J. B. et al. A general method to fine-tune fluorophores for live-cell and in vivo imaging. *Nat. Methods* **14**, 987–994 (2017).
19. Grimm, J. B. et al. A general method to optimize and functionalize red-shifted rhodamine dyes. *Nat. Methods* **17**, 815–821 (2020).
20. Grimm, J. B. et al. A general method to improve fluorophores using deuterated auxochromes. *JACS Au* **1**, 690–696 (2021).
21. DeNardo, L. & Luo, L. Genetic strategies to access activated neurons. *Curr. Opin. Neurobiol.* **45**, 121–129 (2017).
22. Wu, Q. et al. The temporal pattern of cfos activation in hypothalamic, cortical, and brainstem nuclei in response to fasting and refeeding in male mice. *Endocrinology* **155**, 840–853 (2014).
23. Sherin, J. E., Shiromani, P. J., McCarley, R. W. & Saper, C. B. Activation of ventrolateral preoptic neurons during sleep. *Science* **271**, 216–219 (1996).
24. Gammie, S. C. & Nelson, R. J. cFOS and pCREB activation and maternal aggression in mice. *Brain Res.* **898**, 232–241 (2001).
25. Haller, J., Tóth, M., Halasz, J. & De Boer, S. F. Patterns of violent aggression-induced brain c-fos expression in male mice selected for aggressiveness. *Physiol. Behav.* **88**, 173–182 (2006).
26. Josselyn, S. A. & Tonegawa, S. Memory engrams: recalling the past and imagining the future. *Science* **367**, eaaw4325 (2020).
27. Das, A. T., Tenenbaum, L. & Berkhout, B. Tet-On systems for doxycycline-inducible gene expression. *Curr. Gene Ther.* **16**, 156–167 (2016).
28. Amemiya, T., Kambe, T., Fukumori, R. & Kubo, T. Role of protein kinase Cβ in phorbol ester-induced c-fos gene expression in neurons of normotensive and spontaneously hypertensive rat brains. *Brain Res.* **1040**, 129–136 (2005).
29. Iwamoto, M., Björklund, T., Lundberg, C., Kirik, D. & Wandless, T. J. A general chemical method to regulate protein stability in the mammalian central nervous system. *Chem. Biol.* **17**, 981–988 (2010).
30. Miyamae, Y., Chen, L.-C., Utsugi, Y., Farrants, H. & Wandless, T. J. A method for conditional regulation of protein stability in native or near-native form. *Cell Chem. Biol.* **27**, 1573–1581 (2020).
31. Liu, Q. & Tucker, C. L. Engineering genetically-encoded tools for optogenetic control of protein activity. *Curr. Opin. Chem. Biol.* **40**, 17–23 (2017).
32. Hertel, F. & Zhang, J. Monitoring of post-translational modification dynamics with genetically encoded fluorescent reporters. *Biopolymers* **101**, 180–187 (2014).
33. Specht, E. A., Braselmann, E. & Palmer, A. E. A critical and comparative review of fluorescent tools for Live-Cell Imaging. *Annu. Rev. Physiol.* **79**, 93–117 (2017).
34. Linghu, C. et al. Recording of cellular physiological histories along optically readable self-assembling protein chains. *Nat. Biotechnol.* https://doi.org/10.1038/s41587-022-01586-7 (2022).
35. Tomasello, G., Armenia, I. & Molla, G. The Protein Imager: a full-featured online molecular viewer interface with server-side HQ-rendering capabilities. *Bioinformatics* **36**, 2909–2911 (2020).

https://doi.org/10.1038/s41587-022-01524-7

# Methods

## Cloning and molecular biology

All iPAK4 constructs were cloned into a second-generation lentiviral backbone (Addgene, 136636) with either a cytomegalovirus (CMV) or a cFos promoter (Addgene, 47907) using standard Gibson assembly[36]. In brief, the vector was linearized by double digestion (BamHI and EcoRI for CMV-driven constructs; PacI and EcoRI for cFos-driven constructs) and purified by the GeneJET gel extraction kit (Thermo Fisher Scientific). Gene fragments and cFos promoter were generated by polymerase chain reaction (PCR) amplification and then combined with the linearized backbones by Gibson ligation. EGFP-iPAK4 was a gift from B. Cui (Stanford), and HT was cloned from pCAG-Voltron (Addgene, 119033). The eGFP and iPAK4 were connected with an SGGS linker, whereas the HT and iPAK4 were connected with an SGS linker. All plasmids were verified by full sequencing around the cloned regions. The plasmids used in this work are listed in Table 1 and are available on Addgene.

**Table 1 | Plasmids used in this work**

| Plasmid ID | Description | Addgene ID |
|---|---|---|
| DL015: CMV::iPAK4 | iBox-PAK4cat (iPAK4) fusion with CMV promoter, cloned into a lentivirus backbone | 177880 |
| DL016: CMV::eGFP-iPAK4 | eGFP-IPAK4 fusion with CMV promoter, cloned into a lentivirus backbone | 177881 |
| DL017: CMV::HaloTag-iPAK4 | HT-iPAK4 fusion with CMV promoter, cloned into a lentivirus backbone | 177882 |
| DL033: cFos::eGFP-iPAK4 | eGFP-iPAK4 fusion with cFos promoter, cloned into a lentivirus backbone | 177883 |
| DL034: cFos::HaloTag-iPAK4 | HaloTag-iPAK4 fusion with cFos promoter, cloned into a lentivirus backbone | 177884 |
| DL145: TRE::iPAK4 | Tet-On inducible expression of iPAK4 in a lentiviral backbone | 187445 |
| DL146: TRE::eGFP-iPAK4 | Tet-On inducible expression of eGFP-iPAK4 in a lentiviral backbone | 187446 |
| DL147: TRE::HaloTag-iPAK4 | Tet-On inducible expression of HaloTag-iPAK4 in a lentiviral backbone | 187447 |

## Synthesis of $JFX_{608}$-HT

**General synthetic methods.** Commercial reagents were obtained from reputable suppliers and used as received. All solvents were purchased in septum-sealed bottles stored under an inert atmosphere. All reactions were sealed with septa through which a nitrogen atmosphere was introduced unless otherwise noted. Reactions were conducted in round-bottom flasks or septum-capped crimp-top vials containing Teflon-coated magnetic stir bars. Heating of reactions was accomplished with a silicon oil bath or an aluminum reaction block on top of a stirring hotplate equipped with an electronic contact thermometer to maintain the indicated temperatures. Reactions were monitored by thin layer chromatography (TLC) on pre-coated TLC glass plates (silica gel 60 $F_{254}$, 250-µm thickness) or by liquid chromatography–mass spectrometry (LC/MS) (Phenomenex Kinetex 2.1 mm × 30 mm 2.6-µm C18 column; 5-µl injection; 5–98% MeCN/$H_2O$, linear gradient, with constant 0.1% v/v $HCO_2H$ additive; 6-minute run; 0.5 ml $min^{-1}$ flow; electrospray ionization (ESI); positive ion mode). TLC chromatograms were visualized by UV illumination or developed with *p*-anisaldehyde, ceric ammonium molybdate or $KMnO_4$ stain. Reaction products were purified by flash chromatography on an automated purification system using pre-packed silica gel columns or by preparative high-performance liquid chromatography (HPLC) (Phenomenex Gemini NX 30 × 150 mm 5-µm C18 column). Analytical HPLC analysis was performed with an Agilent Eclipse XDB 4.6 × 150 mm 5-µm C18 column under the indicated conditions. High-resolution mass spectrometry was performed by the High Resolution Mass Spectrometry Facility at the University of Iowa. Nuclear magnetic resonance (NMR) spectra were recorded on a 400-MHz spectrometer. $^1H$ and $^{13}C$ chemical shifts were referenced to tetramethylsilane (TMS) or residual solvent peaks. Data for $^1H$ NMR spectra are reported as follows: chemical shift (δ ppm), multiplicity (s = singlet, d = doublet, t = triplet, q = quartet, dd = doublet of doublets, m = multiplet), coupling constant (Hz), integration. Data for $^{13}C$ NMR spectra are reported by chemical shift (δ ppm) with hydrogen multiplicity (C, CH, $CH_2$, $CH_3$) information obtained from distortionless enhancement by polarizition transfer (DEPT) spectra.

**6-*tert*-butoxycarbonyl-$JFX_{608}$ (2).** A vial was charged with 6-*tert*-butoxycarbonyl-carbofluorescein ditriflate[18] (**1**; 250 mg, 0.346 mmol), $Pd_2dba_3$ (31.7 mg, 34.6 µmol, 0.1 eq), XPhos (49.5 mg, 0.104 mmol, 0.3 eq) and $Cs_2CO_3$ (316 mg, 0.969 mmol, 2.8 eq). The vial was sealed and evacuated/backfilled with nitrogen (3×). Dioxane (2 ml) was added, and the reaction was flushed again with nitrogen (3×). After the addition of azetidine-2,2,3,3,4,4-$d_6$ (52.4 mg, 0.830 mmol, 2.4 eq), the reaction was stirred at 100 °C for 4 hours. It was subsequently cooled to room temperature, filtered through Celite with $CH_2Cl_2$ and concentrated to dryness. Purification by silica gel chromatography (20–100% EtOAc/hexanes, linear gradient) afforded 6-*tert*-butoxycarbonyl-$JFX_{608}$ (**2**) as a blue-green solid (181 mg, 95%). $^1H$ NMR ($CDCl_3$, 400 MHz) δ 8.14 (dd, *J* = 8.0, 1.3 Hz, 1H), 8.00 (dd, *J* = 8.0, 0.8 Hz, 1H), 7.62 (dd, *J* = 1.2, 0.7 Hz, 1H), 6.58 (d, *J* = 2.4 Hz, 2H), 6.54 (d, *J* = 8.6 Hz, 2H), 6.21 (dd, *J* = 8.6, 2.3 Hz, 2H), 1.83 (s, 3H), 1.73 (s, 3H), 1.53 (s, 9H); $^{13}C$ NMR ($CDCl_3$, 101 MHz) δ 170.2 (C), 164.6 (C), 155.6 (C), 152.5 (C), 146.8 (C), 137.8 (C), 130.3 (C), 130.1 (CH), 128.9 (CH), 125.1 (CH), 124.8 (CH), 119.8 (C), 110.5 (CH), 108.0 (CH), 88.8 (C), 82.3 (C), 38.5 (C), 35.5 ($CH_3$), 32.8 ($CH_3$), 28.2 ($CH_3$); analytical HPLC: $t_R$ = 13.3 minutes, >99% purity (10–95% MeCN/$H_2O$, linear gradient, with constant 0.1% v/v trifluoroacetic acid (TFA) additive; 20-minute run; 1 ml $min^{-1}$ flow; ESI; positive ion mode; detection at 600 nm); high-resolution mass spectrometry (HRMS) (ESI) calculated for $C_{34}H_{25}D_{12}N_2O_4$ $[M+H]^+$ 549.3501 found 549.3503.

**6-carboxy-$JFX_{608}$ (3).** 6-*tert*-Butoxycarbonyl-$JFX_{608}$ (**2**; 310 mg, 0.565 mmol) was taken up in $CH_2Cl_2$ (10 ml), and TFA (2 mL) was added. The reaction was stirred at room temperature for 6 hours. Toluene (10 ml) was added, and the reaction mixture was concentrated to dryness and then azeotroped with MeOH three times to provide 6-carboxy-$JFX_{608}$ (**3**) as a dark-blue solid (323 mg, 94%, TFA salt). Analytical HPLC and NMR indicated that the material was >95% pure and did not require further purification before amide coupling. $^1H$ NMR ($CD_3OD$, 400 MHz) δ 8.36–8.27 (m, 2H), 7.86–7.78 (m, 1H), 6.91 (d, *J* = 9.1 Hz, 2H), 6.81 (d, *J* = 2.3 Hz, 2H), 6.38 (dd, *J* = 9.1, 2.3 Hz, 2H), 1.82 (s, 3H), 1.70 (s, 3H); $^{13}C$ NMR ($CD_3OD$, 101 MHz) δ 168.0 (C), 167.5 (C), 158.0 (C), 157.0 (C), 139.5 (C), 137.6 (CH), 136.2 (C), 135.5 (C), 132.4 (CH), 132.3 (CH), 131.4 (CH), 121.8 (C), 111.9 (CH), 109.7 (CH), 42.8 (C), 35.6 ($CH_3$), 32.0 ($CH_3$); analytical HPLC: $t_R$ = 10.5 minutes, >99% purity (10–95% MeCN/$H_2O$, linear gradient, with constant 0.1% v/v TFA additive; 20-minute run; 1 ml $min^{-1}$ flow; ESI; positive ion mode; detection at 600 nm); HRMS (ESI) calculated for $C_{30}H_{17}D_{12}N_2O_4$ $[M+H]^+$ 493.2875 found 493.2873.

**$JFX_{608}$-NHS (4).** 6-carboxy-$JFX_{608}$ (**3**, TFA salt; 125 mg, 0.206 mmol) was combined with DSC (116 mg, 0.453 mmol, 2.2 eq) in DMF (5 ml). After adding $Et_3N$ (172 µl, 1.24 mmol, 6 eq) and DMAP (2.5 mg, 20.6 µmol, 0.1 eq), the reaction was stirred at room temperature for 30 minutes. It was subsequently diluted with 10% w/v citric acid and extracted with

EtOAc (2×). The combined organic extracts were washed with water and brine, dried over anhydrous $MgSO_4$, filtered and concentrated in vacuo. Flash chromatography (25–100% EtOAc/$CH_2Cl_2$, linear gradient) yielded 116 mg (95%) of $JFX_{608}$-NHS (**4**) as a dark-blue-green solid. $^1H$ NMR ($CDCl_3$, 400 MHz) δ 8.30 (dd, $J$ = 8.0, 1.4 Hz, 1H), 8.11 (dd, $J$ = 8.0, 0.8 Hz, 1H), 7.78 (dd, $J$ = 1.4, 0.7 Hz, 1H), 6.57 (d, $J$ = 2.4 Hz, 2H), 6.50 (d, $J$ = 8.6 Hz, 2H), 6.23 (dd, $J$ = 8.5, 2.4 Hz, 2H), 2.87 (s, 4H), 1.83 (s, 3H), 1.71 (s, 3H); analytical HPLC: $t_R$ = 11.1 minutes, >99% purity (10–95% MeCN/$H_2O$, linear gradient, with constant 0.1% v/v TFA additive; 20-minute run; 1 ml $min^{-1}$ flow; ESI; positive ion mode; detection at 600 nm); HRMS (ESI) calculated for $C_{34}H_{20}D_{12}N_3O_6$ $[M+H]^+$ 590.3039 found 590.3043.

**$JFX_{608}$-HT ligand (6).** $JFX_{608}$-NHS (**4**; 50 mg, 84.8 µmol) and 2-(2-((6-chlorohexyl)oxy)ethoxy)ethanamine (**5**, 'HaloTag(O2)amine', TFA salt; 43.0 mg, 0.127 mmol, 1.5 eq) were combined in DMF (3 ml), and DIEA (44.3 µl, 0.254 mmol, 3 eq) was added. After stirring the reaction at room temperature for 1 hour, it was diluted with saturated $NaHCO_3$ and extracted with EtOAc (2×). The combined organic extracts were washed with water and brine, dried over anhydrous $MgSO_4$, filtered and concentrated in vacuo. Purification of the crude product by silica gel chromatography (50–100% EtOAc/toluene, linear gradient) provided $JFX_{608}$-HT ligand (**6**) as a blue foam (47 mg, 79%). $^1H$ NMR ($CDCl_3$, 400 MHz) δ 8.02 (dd, $J$ = 8.0, 0.7 Hz, 1H), 7.94 (dd, $J$ = 7.9, 1.4 Hz, 1H), 7.44–7.39 (m, 1H), 6.73 (t, $J$ = 4.8 Hz, 1H), 6.57 (d, $J$ = 2.4 Hz, 2H), 6.52 (d, $J$ = 8.6 Hz, 2H), 6.20 (dd, $J$ = 8.6, 2.4 Hz, 2H), 3.64–3.56 (m, 6H), 3.54–3.48 (m, 4H), 3.38 (t, $J$ = 6.6 Hz, 2H), 1.83 (s, 3H), 1.78–1.73 (m, 2H), 1.72 (s, 3H), 1.55–1.48 (m, 2H), 1.45–1.38 (m, 2H), 1.34–1.27 (m, 2H); analytical HPLC: $t_R$ = 12.6 minutes, >99% purity (10–95% MeCN/$H_2O$, linear gradient, with constant 0.1% v/v TFA additive; 20-minute run; 1 ml $min^{-1}$ flow; ESI; positive ion mode; detection at 600 nm); HRMS (ESI) calculated for $C_{40}H_{37}D_{12}ClN_3O_5$ $[M+H]^+$ 698.4108 found 698.4118.

### Fiber expression in HEK cells

HEK293T cells (American Type Culture Collection (ATCC), CRL-11268) were grown and split following standard protocols as described previously[37]. HEK cells at low passage number (<10 passages) were plated at a confluence of 30% onto 10-cm dishes coated with gelatin (STEMCELL Technologies, 07903) or 14-mm glass-bottom dishes (CellVis, D35-14-1.5-N) coated with 40 µg $ml^{-1}$ poly-L-lysine (P8920, Sigma-Aldrich). DMEM supplemented with 10% FBS and penicillin–streptomycin was used as the culture medium. Cells were grown at 37 °C and 5% $CO_2$.

When cells reached 50–70% confluence, genes were delivered by either lentivirus or TransIT-293 (Mirus, MIR2700) transfection kit. In lentiviral transduction, the high-titer lentiviral vectors were first pre-mixed at the designated ratio and diluted to 10% of the initial concentration by DMEM medium. The cells' culture medium was then replaced by the fresh lentivirus-containing DMEM medium, and the cells were further incubated at 37 °C and 5% $CO_2$ for ~24 hours. In the TransIT-293 transfection, 1 µg of plasmids at the designated ratio were first diluted by 100 µl of Opti-MEM medium, followed by the addition of 3 µl of TransIT-293 reagent. The cocktail was incubated at room temperature for 15 minutes and diluted ten-fold into DMEM on the culture dishes. The cells were then further incubated at 37 °C and 5% $CO_2$ for ~24 hours.

### Fiber labeling

The in cellulo fibers were labeled with HT ligand JF dyes. In this work, the cell-permeable dyes were $JF_{503}$, $JF_{525}$, $JF_{552}$, $JFX_{608}$ and $JF_{669}$. The JF dyes were first diluted into 1 mM stock solution as described previously[17], which was aliquoted and stored at −20 °C. The 1 mM solution was further diluted to 1 µM in 37 °C DMEM medium for HEK cells or BPNM/SM1 medium for neurons. The dyed medium was used to replace the original medium in the culture dishes at timed staining. In the dye switching processes, the medium containing the original dye was fully removed, followed by thorough wash of the culture dishes five times with 37 °C culture medium. Then, the medium with 1 µM new dye was added to the cells, and the cells were returned to the incubator at 37 °C and 5% $CO_2$.

### Measurements of HT dye labeling kinetics in HEK cells

HEK cells were transfected with an inducible nuclear-localized HT protein (HT-NLS, Addgene, 82518). DOX (2 µg $ml^{-1}$) was added 12 hours after transfection to induce the expression of HT-NLS. Twenty-four hours after transfection, cells were incubated with 0.1 µM of the indicated dye, and nuclear fluorescence was monitored via wide-field epifluorescence microscopy as a function of time.

### Primary neuron culture

All procedures involving animals were in accordance with the US National Institutes of Health *Guide for the Care and Use of Laboratory Animals* and were approved by the Institutional Animal Care and Use Committee at Harvard University.

Before the plating of primary hippocampal neurons, 14-mm glass-bottom dishes were first incubated with 40 µg $ml^{-1}$ of poly-D-lysine (PDL) in PBS at room temperature for 1 hour and subsequentially with 20 µg $ml^{-1}$ of laminin (Thermo Fisher Scientific, 23-017-015) at 4 °C overnight, followed by thorough wash with PBS. Hippocampi (BrainBits, SKU, SDEHP) from embryonic day 18 (E18) rats were dissected and resuspended in BrainPhys medium (BPNM, STEMCELL Technologies, 05790) supplemented with 2% SM1 (STEMCELL Technologies, 05792), 5 mM L-glutamine (STEMCELL Technologies, 07100) and 35 µg $ml^{-1}$ of L-glutamic acid (Sigma-Aldrich, 49449), to a final concentration of $3.0 \times 10^6$ cells per milliliter. The neurons were then plated at a density of 30,000 cells per $cm^2$ on the pre-treated glass-bottom dishes, with subsequent addition of 2 ml of BPNM with 2% SM1 (BPNM/SM1). Neuronal health was monitored daily from days in vitro 1 (DIV1) to DIV7. Every 3–4 days, 1 ml of the medium in each dish was replaced with 37 °C fresh BPNM/SM1 medium.

### Patch-clamp electrophysiology

Whole-cell recordings were performed in extracellular buffer containing (in mM): 125 NaCl, 2.5 KCl, 15 HEPES, 25 D-glucose, 1 $MgCl_2$ and 2 $CaCl_2$ (pH 7.2–7.3 with NaOH). Fiber-forming and non-forming (control) neurons were visualized with a home-built inverted epifluorescence microscope. Experiments were made at 23 °C under ambient atmosphere. The whole-cell internal solution comprised (in mM): 8 NaCl, 130 $KMeSO_3$, 10 HEPES, 5 KCl, 0.5 EGTA, 4 Mg-ATP and 0.3 $Na_3$-GTP. The pH was adjusted to 7.2–7.3 with KOH, and osmolarity was set to 290–295 mOsm $L^{-1}$. Borosilicate glass pipettes were used with a resistance of 3–5 MΩ (1.5 mm optical density (OD)). Signals were acquired and filtered at 4 kHz with the internal Bessel filter using a Multiclamp 700B (Molecular Devices) and digitized with PCIe-6323 (National Instruments) at 10 kHz. After the whole-cell configuration, membrane capacitance ($C_m$) and membrane resistance ($R_m$) were estimated under voltage-clamp mode. Measurements of resting membrane potential ($V_{rest}$), rheobase and spike rates were made under current-clamp mode. Rheobase was defined as the minimum current step (in 500-ms duration) required for any spike onset. Whole-cell recordings were monitored and analyzed using a custom code written in LabView and MATLAB.

### Lentivirus production

**Lentivirus production in HEK cells.** Plasmids of CMV::iPAK4, CMV::HaloTag-iPAK4 and cFos::eGFP-iPAK4 were used to produce lentivirus according to published methods[38]. In brief, low-passage-number HEK293T cells (ATCC, CRL-11268) were plated onto gelatin-coated (STEMCELL Technologies, 07903) 10-cm dishes. When HEK cells reached 80% confluence, the medium was exchanged to a serum-free DMEM. After 0.5–1 hours, cells were transfected using polyethylenimine (PEI; Sigma-Aldrich, 408727). Then, 7 µg of the vector plasmid, 4 µg of the second-generation packaging plasmid psPAX2 (Addgene,

12260) and 2 µg of viral entry protein VSV-G plasmid pMD2.G (Addgene, 12259) were mixed into 600 µl of serum-free DMEM, and 20 µl of 1 mg ml$^{-1}$ PEI was then added. The mixture was incubated at room temperature for 15 minutes and added dropwise to the plate. After 3–4 hours, the medium was exchanged back to 10 ml of DMEM10. The supernatant was harvested at 36 hours after transfection, and another 10 ml of DMEM10 was added to the cells and incubated for another 24 hours. At 60 hours after transfection, the supernatant was harvested again and combined with the first batch of supernatant, centrifuged for 5 minutes at 500*g* and filtered through a 0.45-µm filter (EMD Millipore, SE1M003M00).

**Lentivirus concentration.** Next, 1 part of Lenti-X concentrator (TaKaRa, 631232) was first mixed with 3 parts of supernatant and incubated at 4 °C overnight for lentivirus precipitation. The mixture was then centrifuged at 1,500*g* for 45 minutes at 4 °C. The supernatant was gently removed, and the off-white pellet was resuspended in 200 µl of neurobasal-based medium. The concentrated virus was titrated in neurons, aliquoted and stored at −80 °C for neuronal transduction.

### Fiber expression in neurons

Genes were delivered to neurons by lentiviral transduction at DIV7–10. The lentiviral vectors of CMV::iPAK4, CMV::HaloTag-iPAK4 and cFos::eGFP-iPAK4 were first mixed at the designated ratio, which was further diluted to 10% of the original concentration by fresh BPNM/SM1 medium. The dilution was then used to replace the original medium in neuronal culture. The neurons were incubated in the lentivirus-containing medium at 37 °C and 5% $CO_2$ for 12 hours, followed by medium replacement with lentivirus-free medium.

### Chemical activation of neuronal activity

The cFos promoter was activated by PMA (Sigma-Aldrich, P8139). In brief, the PMA was first diluted with DMSO to form a 1 mM stock solution. At the designated time, 2 µl of PMA stock was directly added to each 14-mm glass-bottom culture dish, which contained 2 ml of BPNM/SM1 medium. The dishes were then stirred gently to mix the PMA and medium. After PMA addition, the dishes were returned to an incubator at 37 °C with 5% $CO_2$.

### Multi-spectral imaging

Multi-spectral images were acquired using a Zeiss LSM 980 confocal microscope with Airyscan 2. Lambda scan mode was used to image fibers with multi-color labeling. The excitation laser wavelengths were 488 nm (eGFP, $JF_{503}$ and $JF_{525}$), 561 nm ($JF_{552}$ and $JFX_{608}$) and 639 nm ($JF_{669}$). In each Lambda scan, 32 channels in the range of 414–688 nm were simultaneously acquired to obtain a hyper-spectral stack of images. The images were then unmixed with the built-in linear unmixing algorithm in Zen Blue software. Reference images of individual fluorescent labels were taken in the same instrumental configuration to train the linear unmixing algorithm. The spectral unmixing typically produced negligible residual signals.

### Time-lapse microscopy

HEK cells expressing the target constructs were grown on 14-mm glass-bottom culture dishes (CellVis, D35-14-1.5-N) and monitored under Zeiss Elyra7 or Discoverer7 microscopes with 488-nm laser and a ×10 air objective in an environmental chamber at 37 °C and 5% $CO_2$. Images were acquired at 1% laser power, 300-ms exposures and 10-minute intervals over 10–23 hours after transfection.

### Image processing and data analysis

MATLAB and ImageJ were used for image processing. Images of individual fibers were rotated to align the long axis to the *x*-axis. Fluorescence profiles were then calculated as the median fluorescence in each spectral channel across the width of the fiber. Fibers that were not in focus or where two or more fibers crossed each other near a dye transition were excluded from analysis. Dye transitions were identified as local maxima in the second derivative of the dye fluorescence as a function of position. To avoid spurious peaks due to noise, the second derivative signal was smoothed with a kernel of typically 10 minutes, although this smoothing was omitted when calculating the width of the dye transition (Supplementary Fig. 3a).

For tracking fibers during time-lapse recordings, a region of interest (ROI) was manually defined on a maximum intensity projection of the image stack, to select individual fibers and to encompass the entire fiber in all frames of the movie. A Radon transform was then calculated on the selected ROI for each video frame. The peak of the Radon transform was associated with the fiber. The corresponding line in the real-space movie was used to calculate the fiber intensity profile. Nearby parallel lines on either side of the fiber were averaged and used for background subtraction. The fiber ends were then found by applying a simple threshold to the plot of fluorescence versus position. The fluorescence of the cytoplasm was determined by summing the intensity from pixels that were on-cell but off-fiber. Fiber length trajectories were median filtered (kernel = 1 hour) to suppress small, high-frequency fluctuations caused by segmentation noise.

### Statistics and reproducibility

All statistical tests performed are specified in the figure legends. Differences with values of $P < 0.05$ were considered statistically significant. Sample sizes are also specified in the figure legends. Two-sided Student's *t*-test was applied for statistical comparison of two groups. The fluorescence images presented in the manuscript, including Figs. 1d, 2b,d, 3b,c, 4c and 5a,d,g and Supplementary Figs. 1a, 4a,b, 5a–d, 7b–e, 9a–f, 10b, 11c, 13a, 14b, 15 and 16a,b, are representative images from at least three independent repeats.

### Reporting summary

Further information on research design is available in the Nature Research Reporting Summary linked to this article.

## Data availability

Data comprising images and time-lapse recordings of iPAK4 fibers, as well as patch-clamp recordings, are available from the corresponding authors upon reasonable request.

## References

36. Gibson, D. G. et al. Enzymatic assembly of DNA molecules up to several hundred kilobases. *Nat. Methods* **6**, 343–345 (2009).
37. Thomas, P. & Smart, T. G. HEK293 cell line: a vehicle for the expression of recombinant proteins. *J. Pharmacol. Toxicol. Methods* **51**, 187–200 (2005).
38. Geraerts, M., Michiels, M., Baekelandt, V., Debyser, Z. & Gijsbers, R. Upscaling of lentiviral vector production by tangential flow filtration. *J. Gene Med.* **7**, 1299–1310 (2005).

## Acknowledgements

We thank D. Kim, Y. Baskaran and E. Manser for helpful discussions. We thank B. Cui for the PAK4 plasmid and C. Hellriegel at the Harvard Center for Biological Imaging for assistance with microscopy. We thank S. Begum, A. Preecha and J. Koob for technical assistance. This work was supported by Schmidt Futures (A.E.C., X.L., E.M., P.P. and B.T.), a Vannevar Bush Faculty Fellowship (A.E.C.), the Howard Hughes Medical Institute (A.E.C., J.B.G., N.F., L.D.L., H.S. and D.B.), National Institutes of Health grant 1-R21-1EY033669 (A.E.C., D.L. and X.L.), a John S. LaDue Fellowship (B.Z.J.) and the Harvard Brain Science Initiative (D.L.).

## Author contributions

D.L. and A.E.C. conceived the project and designed the experiments. D.L. and X.L. cloned the plasmids. P.P. and D.L.

performed the patch-clamp measurements. D.L. and X.L. performed the time-lapse imaging in HEK cells. D.L. performed all other characterizations in cultured cells and acquired the imaging data. E.M. analyzed data and prepared figures. B.Z.J. helped with experiments for the revisions. J.B.G., N.F. and L.D.L. synthesized and supplied the JF dyes. H.S. and D.B. assisted in protein design and optimization. D.L., A.E.C., P.P. and B.T. analyzed the data. D.L. and A.E.C. wrote the paper. All authors participated in the revision of the manuscript.

## Competing interests

A.E.C., D.L. and X.L. have filed a US patent application on protein-based ticker tapes for intracellular recordings. The remaining authors declare no competing interests.

## Additional information

**Supplementary information** The online version contains supplementary material available at https://doi.org/10.1038/s41587-022-01524-7.

**Correspondence and requests for materials** should be addressed to Dingchang Lin or Adam E. Cohen.

**Peer review information** *Nature Biotechnology* thanks Hyongbum Henry Kim, Randall Platt and the other, anonymous, reviewer(s) for their contribution to the peer review of this work.

nature biotechnology

Article

https://doi.org/10.1038/s41587-022-01524-7

# Time-tagged ticker tapes for intracellular recordings

In the format provided by the authors and unedited

**Contents**

**Supplementary Movie Captions**

**Movie S1. Time-lapse recording of iPAK4 fiber growth in HEK293T cells.** HEK293T cells were co-infected with CMV::iPAK4 (90%), CMV::HT-iPAK4 (5%), and CMV::eGFP-iPAK4 (5%) lentiviruses and stained with $JF_{669}$. Time-lapse video microscopy was acquired over 43 h, starting 20 h after lentiviral infection, with one frame every 10 min.

**Movie S2. Tracking individual iPAK4 fibers in HEK293T cells with real-time growth profiles.** Left: Time-lapse movies showing the tracking of single iPAK4 fibers. Right: Real-time growth profiles of the corresponding fibers.

**Movie S3. Time-lapse recording of iPAK4 fiber growth with one dye switch in HEK293T cells.** HEK293T cells co-infected with CMV::iPAK4 (95%) and CMV::HT-iPAK4 (5%) lentiviruses. The dye was switched (from $JF_{552}$ to $JF_{669}$) right before the imaging. Time-lapse video microscopy was acquired over 40 h, starting 20 h after transfection, with one frame every 5 min.

**Movie S4. Time-lapse recording of iPAK4 fiber growth in neurons.** Primary neurons co-infected with CMV::iPAK4 (95%) and CMV::HT-iPAK4 (5%) lentiviruses. Time-lapse video microscopy was acquired over 40 h, starting 20 h after transfection, with one frame every 5 min.

**Movie S5. Tracking individual iPAK4 fibers in primary neurons with real-time growth profiles.** Left: Time-lapse movies showing the tracking of single iPAK4 fibers. Right: Real-time growth profiles of the corresponding fibers.

**Supplementary Calculation 1: Kinetics of iPAK4 fiber growth.**

We first examine the relation between the concentration, *C*, of soluble iPAK4 monomers and the rate of change of the length, *L*, of a fiber. The cross-sectional area is *A* (μm$^2$), the density of molecules in the fiber is $\rho$ (molecules/μm$^3$), the surface density of molecules along the growing tip is $\alpha$ (molecules/μm$^2$), and the linear density along the growth direction is $\lambda$ (molecules/μm). Hence $\rho = \alpha\,\lambda$.

Based on the published crystal structure (PDB:4XBR), the volume of the unit cell is 1.12×10$^6$ Å$^3$ and contains 6 iPAK4 monomers. This corresponds to a monomer density $\rho$ = 5.36 × 10$^6$ molecules/μm$^3$, or equivalently a monomer concentration in the fiber of 8.9 mM.

Steady state fiber growth. The rate of growth of the fiber is related to the rate of decrease of the number of monomers, *n*, from the cytoplasm by:

$$\frac{dn}{dt} = -A\rho\frac{dL}{dt}, \qquad [1]$$

Implying that the rate of change of soluble monomer concentration due to fiber growth is:

$$\frac{dC}{dt} = -\frac{A}{V}\rho\frac{dL}{dt}, \qquad [2]$$

where *V* is the volume of the cytoplasm. For example, growth of a fiber with a diameter *d* = 2 μm at a rate of 1 μm/hr corresponds to incorporation of 4,700 monomers/s. For a cell with a volume of 5 pL, this corresponds to a decrease in soluble monomer concentration (in the absence of replenishment by protein synthesis) of 1.6 nM/s.

Let us further assume that the off-rate of monomers from the fiber is negligible, and that the fiber grows via addition across its entire face. Then the rate of growth of the fiber is:

$$\frac{dL}{dt} = \frac{C}{\lambda}k_{grow}, \qquad [3]$$

where $k_{grow}$ (M$^{-1}$ s$^{-1}$) is the first-order rate constant for monomer addition to the fiber. If we include protein synthesis at rate $k_{synth}$ (moles/s) and degradation of soluble proteins at rate $k_{deg}$ (s$^{-1}$), and insert Eq. 3 into Eq. 2, we obtain:

$$\frac{dC}{dt} = \frac{k_{synth}}{V} - k_{deg}C - \frac{A\alpha}{V}Ck_{grow}, \qquad [4]$$

Under steady-state conditions ($\frac{dC}{dt} = 0$), the concentration is

$$C_{ss} = \frac{k_{synth}}{Vk_{deg} + A\alpha k_{grow}}, \qquad [5]$$

and the growth rate is

$$\frac{dL_{ss}}{dt} = \frac{k_{synth}k_{grow}}{V\,\lambda k_{deg} + A\rho k_{grow}}. \qquad [6]$$

Thus at long times, the growth is linear, and the rate is set by the balance of protein synthesis and protein removal from the cytoplasm, either by degradation or incorporation into the fiber.

Time-dependent growth profile. For further analysis we assume that incorporation into the fiber is the only path for removing soluble proteins, i.e. protein degradation is negligible ($k_{deg} \approx 0$). Then

$$C_{ss} = \frac{k_{synth}}{A\,\alpha\,k_{grow}}.$$

Let us assume that fiber nucleation occurs once the soluble concentration reaches a threshold, $C_{nuc}$. Then one can solve explicitly for the time-dependent soluble concentration:

$C(t) = (C_{nuc} - C_{ss})e^{-\frac{A\alpha k_{grow}}{V}t} + C_{ss}$,
and the time-dependent fiber length:

$$L(t) = \frac{k_{grow}}{\lambda} C_{ss} t + \frac{V}{A\rho}(C_{nuc} - C_{ss})\left(1 - e^{-\frac{A\alpha k_{grow}}{V}t}\right), \quad [7a]$$

which can also be written as:

$$L(t) = \frac{k_{synth}}{A\rho} t + \frac{V}{A\rho}(C_{nuc} - C_{ss})\left(1 - e^{-\frac{A\alpha k_{grow}}{V}t}\right). \quad [7b]$$

Eqs. 7a and 7b show that fiber growth has two phases. Initially there is rapid growth driven by the excess soluble monomers in the cytoplasm. Once the cytoplasmic concentration has decreased, the fiber settles into a linear growth mode.

Multi-color labeling. We now consider multi-color labeling of a growing fiber. Consider the case of two HaloTag dyes, *R* (red) and *G* (green), each of which follows a time-dependent intracellular concentration, *R*(*t*) and *G*(*t*), respectively. These profiles are not fully under user control, particularly *in vivo*. A user can specify how much dye is added, and when; but the free dye concentrations in the cytoplasm depend on dye pharmacokinetics: permeation across the cell membrane, metabolism and excretion *in vivo*. Here we will not explicitly simulate these processes, but instead assume that *R*(*t*) and *G*(*t*) are known.

We further assume that the HaloTag labeling reactions are fast compared to all the other dynamics in the system. This assumption is valid for dye concentrations in the μM range, typical of HaloTag labeling experiments *in vivo*. Finally, we assume that the labeling reaction rate constants are the same for the two dyes. If these rate constants differ, the concentrations of the dyes should be replaced by their specific activities.

Under these assumptions, the concentrations of soluble monomers labeled with each color of dye follow the mole fractions of the dyes at the time of protein translation:

$$\frac{dC_R}{dt} = \frac{k_{synth}^{HT}}{V}\frac{R(t)}{R(t)+G(t)} - \frac{k_{deg}^{HT}}{V}C_R - \frac{A\alpha}{V}k_{grow}C_R, \quad [8]$$

$$\frac{dC_G}{dt} = \frac{k_{synth}^{HT}}{V}\frac{G(t)}{R(t)+G(t)} - \frac{k_{deg}^{HT}}{V}C_G - \frac{A\alpha}{V}k_{grow}C_G.$$

Here the HT superscripts indicate that the parameters are for the HaloTag-labeled iPAK4 monomers. We assume that the labeled and unlabeled iPAK4 monomers incorporate into the fiber with the same rate constant, $k_{grow}$.

Both labeled and unlabeled monomers contribute to the growth of the fiber:

$$\frac{dL}{dt} = (C_R + C_G + C_{blank})\frac{k_{grow}}{\lambda}. \quad [9]$$

The color along the fiber is proportional to the concentration of each fluorescently labeled species (we assume that the concentrations of each labeled species are low enough to avoid competition for binding sites in the fiber):

$$R(L(t)) = C_R(t), \text{ and} \quad [10]$$
$$G(L(t)) = C_G(t).$$

We integrated this model with step-function changes in dye concentrations, considering the case where the change in concentration occurred either before or after fiber nucleation (Fig. S2). These results are in good qualitative agreement with our observed fiber fluorescence profiles.

**Supplementary Calculation 2: Effect of iPAK4 fibers on cell membrane surface area and cell volume.**
Let us estimate how much an iPAK4 changes the membrane area of a HEK cell or a neuron. Measurements of membrane capacitance in HEK cells typically give ~10 pF, and our measurements in cultured neurons gave ~60 pF (Fig. 5c(ii)). At a specific capacitance of 1 $\mu F/cm^2$, these capacitance values correspond to surface areas of 1,000 $\mu m^2$ and 6,000 $\mu m^2$, respectively. The membrane forms a sheath around the fibers, so at a typical fiber radius of 1 $\mu m$, the additional membrane area is approximately 6.3 $\mu m^2$ per $\mu m$ of fiber extension beyond the size of the cell. For a fiber that protrudes by 20 $\mu m$, the additional surface area is ~130 $\mu m^2$. This is a modest perturbation on the starting surface area for HEK cells and is negligible for neurons.

We can similarly estimate the volume increases (though the additional volume is largely occupied by fiber). The volume of a HEK cell is ~5,000 $\mu m^3$, and for a cultured neuron the volume is somewhat larger. A 1 $\mu m$-radius fiber poking out of a cell will introduce additional volume of 3.1 $\mu m^3$ per micron of length, so for a fiber that protrudes by 20 $\mu m$, the additional volume is ~62 $\mu m^3$. This is an insignificant increase on the baseline. The axons and dendrites of neurons typically contain vastly larger surface areas and volumes than any fibers poking from the cells.

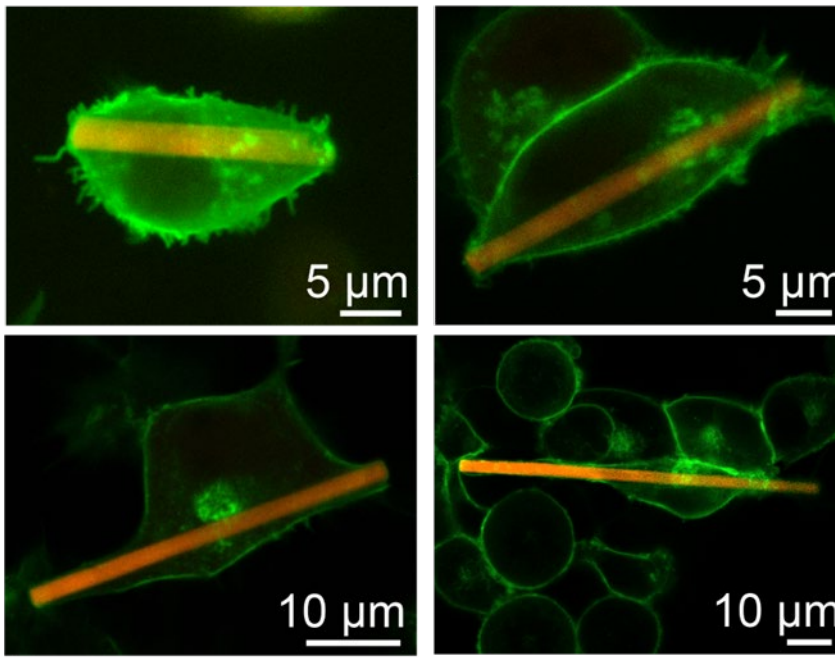


**Figure S1. iPAK4 fiber morphology, nucleation and growth.** Related to Fig. 1. **a**, Images of HEK293T cells expressing CMV::iPAK4 (95%) and CMV::HT-iPAK4 (5%). The fibers were stained with $JFX_{608}$ and the membrane was labeled by expressing GPI-eGFP. In cells where the fiber length exceeded the cell size, the membrane wrapped around the extended fiber.

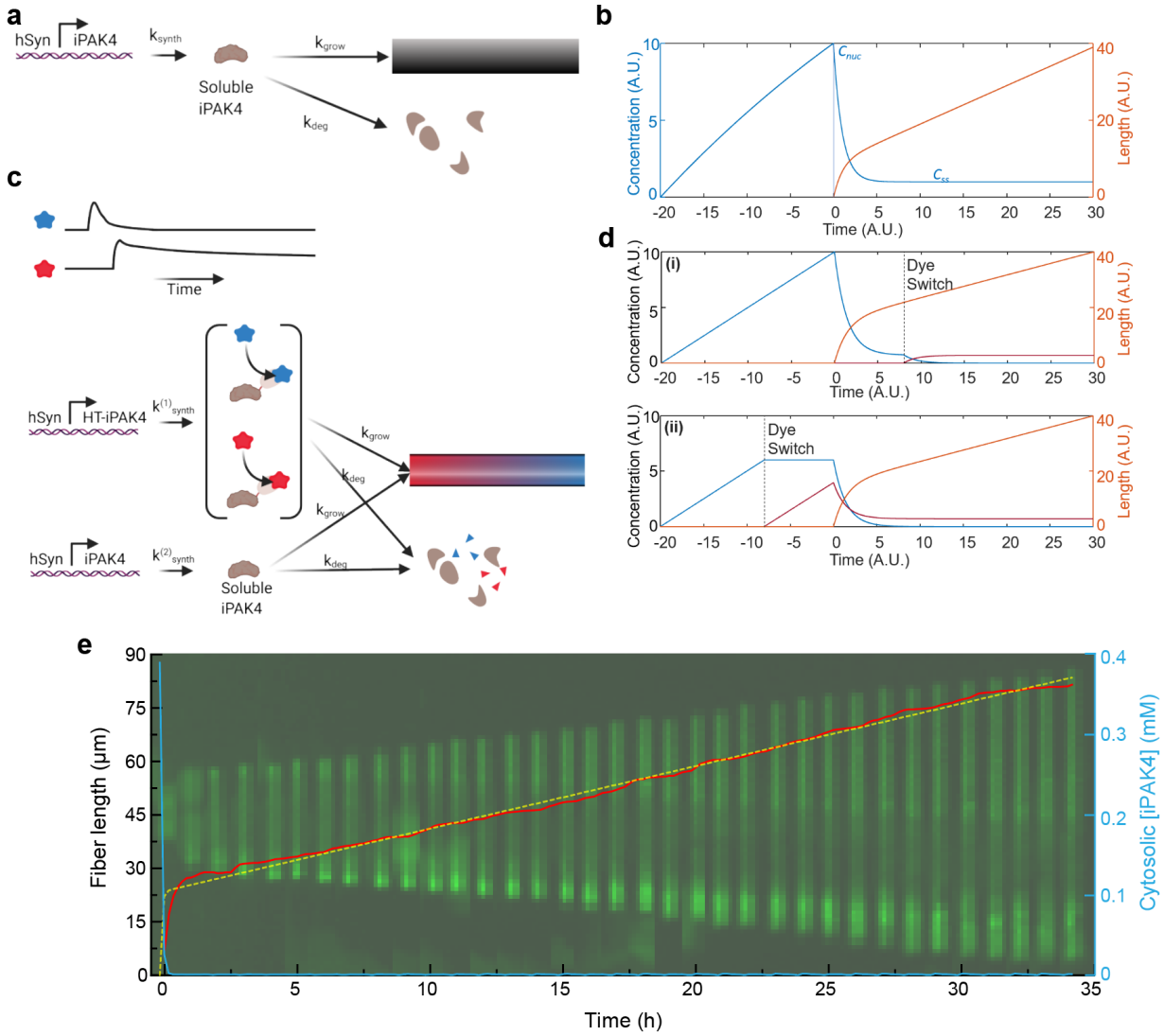


**Figure S2. Model of iPAK4 fiber growth.** Related to Fig. 1 **a**, Kinetic scheme for fiber growth, comprising transcription and translation (here modeled as a single step), protein degradation, and assembly into the fiber. Fiber nucleation is assumed to occur at a critical concentration, $C_{nuc}$. Monomer incorporation into the fiber is assumed to follow first-order kinetics in monomer concentration. **b**, Simulation of fiber nucleation and growth. Initially, monomers accumulate, and monomer synthesis is partially compensated by protein degradation. At $t = 0$ the monomer concentration crosses the nucleation threshold, leading to a period of rapid growth until the monomer concentration reaches a level where protein synthesis and removal via fiber growth are balanced. **c**, Multi-component kinetic model comprising iPAK4 with a HaloTag ligand and bare iPAK4. The labeling ratio of the HT-iPAK4 is proportional to the mole-fraction of each dye at the time of protein translation. **d**, Simulations of fiber growth profiles with a step-wise replacement of one dye for another. (i) Dye switch after fiber nucleation; (ii) dye switch before fiber nucleation. **e**, Representative iPAK4 fiber growth profile (red solid line) and images at key frames (green, background) after the crystal nucleation. Simulated growth profile (yellow dash line) and cytosolic iPAK4 concentration (blue solid line).

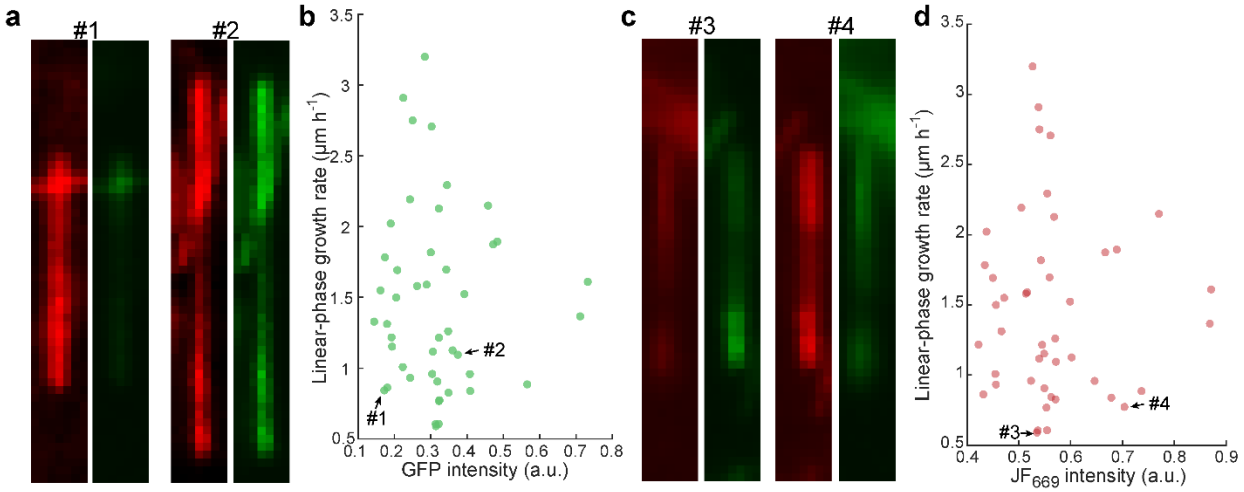


**Figure S3. Fluorescent tags do not affect iPAK4 fiber growth rate.** Related to Fig. 1. **a,** Representative images of two iPAK4 fibers with different amounts of eGFP-iPAK4, taken from the same plate. **b,** Linear-phase growth rate of iPAK4 fibers as a function of the fluorescence intensity of eGFP-iPAK4 in the fiber (*N* = 46 fibers, Pearson *r* = -0.05; p = 0.75). **c,** Representative images of two iPAK4 fibers with different amounts of HT-iPAK4, taken from the same plate. **d,** Linear-phase growth rate of iPAK4 fibers as a function of the fluorescence intensity of HT-iPAK4 in the fiber (*N* = 46 fibers, Pearson *r* = -0.02; p = 0.89).

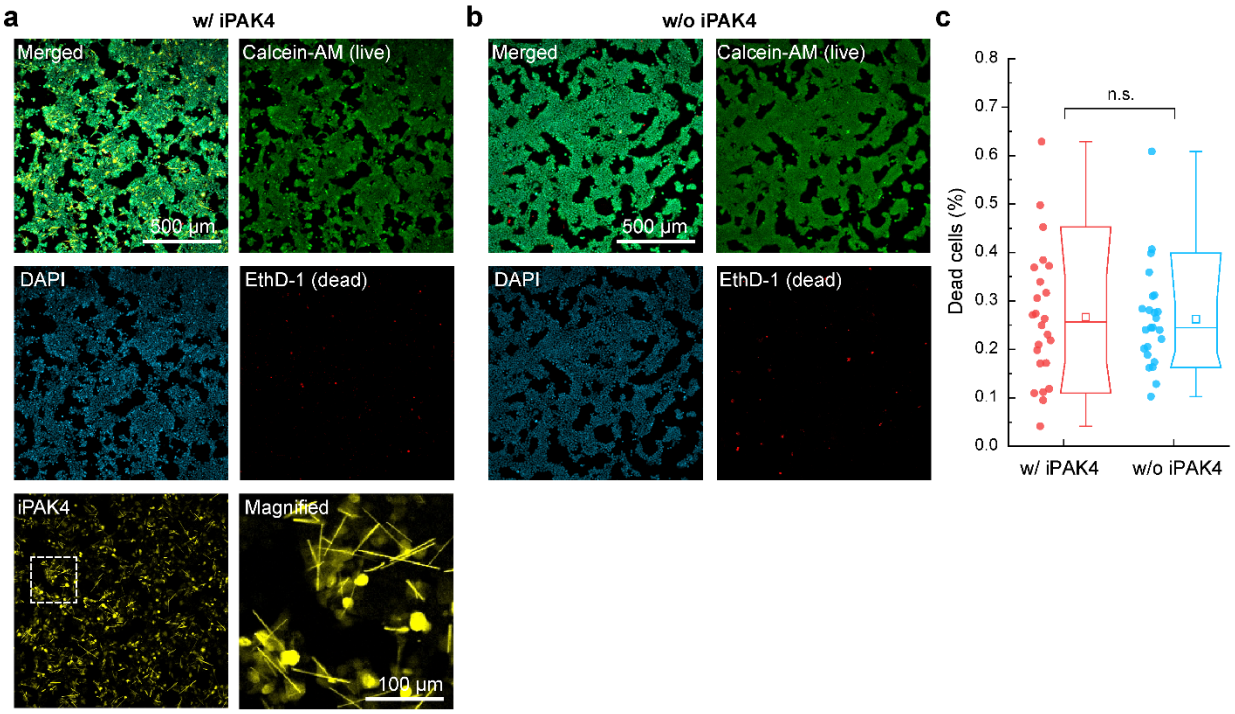


**Figure S4. Live-dead assay to assess effect of iPAK4 fibers on cell health.** Related to Fig. 1. **a**, Images of HEK293T cells expressing CMV::iPAK4 (95%) and CMV::HT-iPAK4 (5%). Many iPAK4 fibers can be identified in a magnified view. **b,** Control group with the same culture conditions but without lentiviral transduction of iPAK4 constructs. Green channel: live cells (calcein-AM); red channel: dead cells (EthD-1); yellow channel: HaloTag-iPAK4 stained with $JFX_{608}$. **c,** Statistical comparison of the dead cell population in iPAK4+ and iPAK4- groups. Each point represents one field of view. Two dishes per condition were investigated. No significant difference was found between the two groups. The statistical comparison was performed by two-sided student's t-test. *N* = 24 fields of view iPAK4+, 24 fields of view iPAK4-. Lower and upper bounds of the box plot: 25th and 75th percentile; lower and upper whiskers: minimum and maximum; squares: mean; center lines: median.

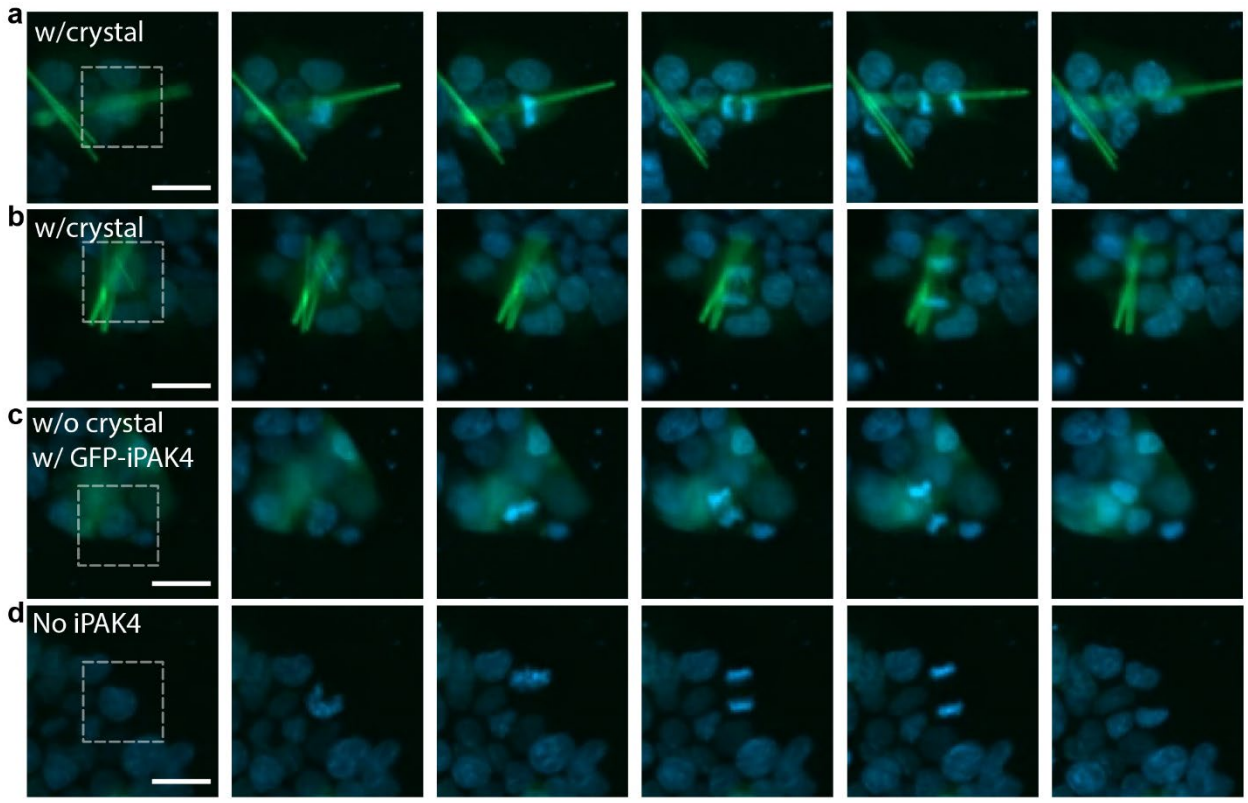


**Figure S5. Mitosis in HEK293T cells containing iPAK4 fibers.** Related to Fig. 1. In all cases, DNA was stained with Hoechst 33342. **a, b,** Snapshots showing mitosis and cell divisions of a HEK293T cell containing an iPAK4 fiber. **c,** A cell expressing iPAK4 and eGFP-iPAK4 but without an iPAK4 fiber. **d,** A cell not expressing iPAK4. In all cases mitosis appeared to proceed normally. Blue: Hoechst 33342 nuclear stain. Green: GFP-iPAK4. Scale bar 20 μm.

**a**

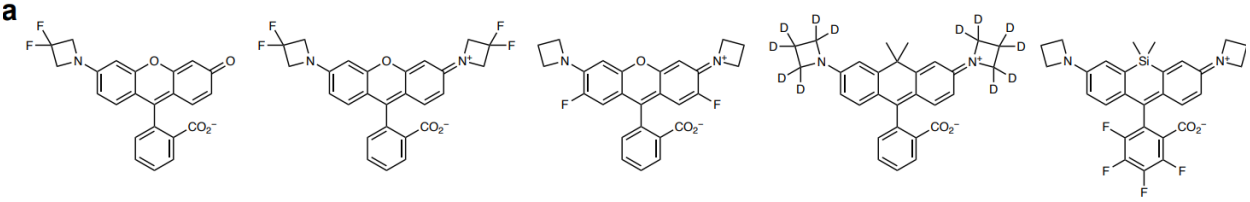

| | $JF_{503}$ | $JF_{525}$ | $JF_{552}$ | $JFX_{608}$ | $JF_{669}$ |
|---|---|---|---|---|---|
| $\lambda_{abs}$ (nm) | 503 | 525 | 552 | 608 | 669 |
| $\varepsilon$ ($M^{-1}cm^{-1}$) | 83,000 | 94,000 | 95,000 | 111,000 | 112,000 |
| $\lambda_{em}$ (nm) | 529 | 549 | 575 | 628 | 682 |
| $\Phi_f$ | 0.87 | 0.91 | 0.83 | 0.74 | 0.37 |

**b**

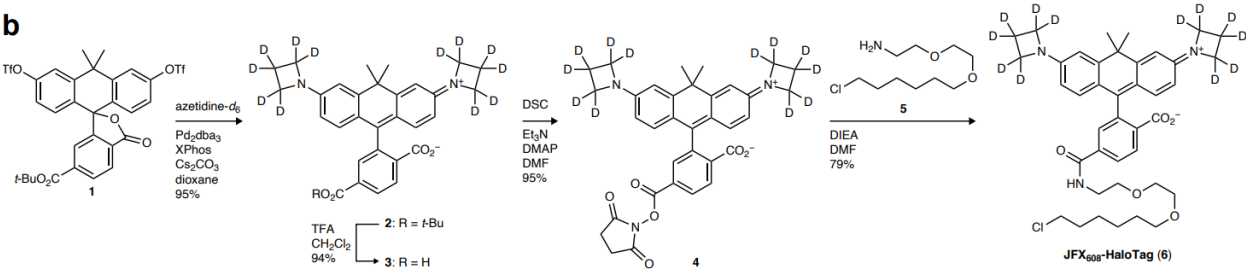


**Figure S6. JaneliaFluor HaloTag ligand dyes used in this study.** Related to Fig. 2. **a**, Chemical structures and spectral properties of the free Janelia Fluor dyes: $JF_{503}$, $JF_{525}$, $JF_{552}$, $JFX_{608}$, and $JF_{669}$. **b**, Synthesis of $JFX_{608}$-HaloTag.

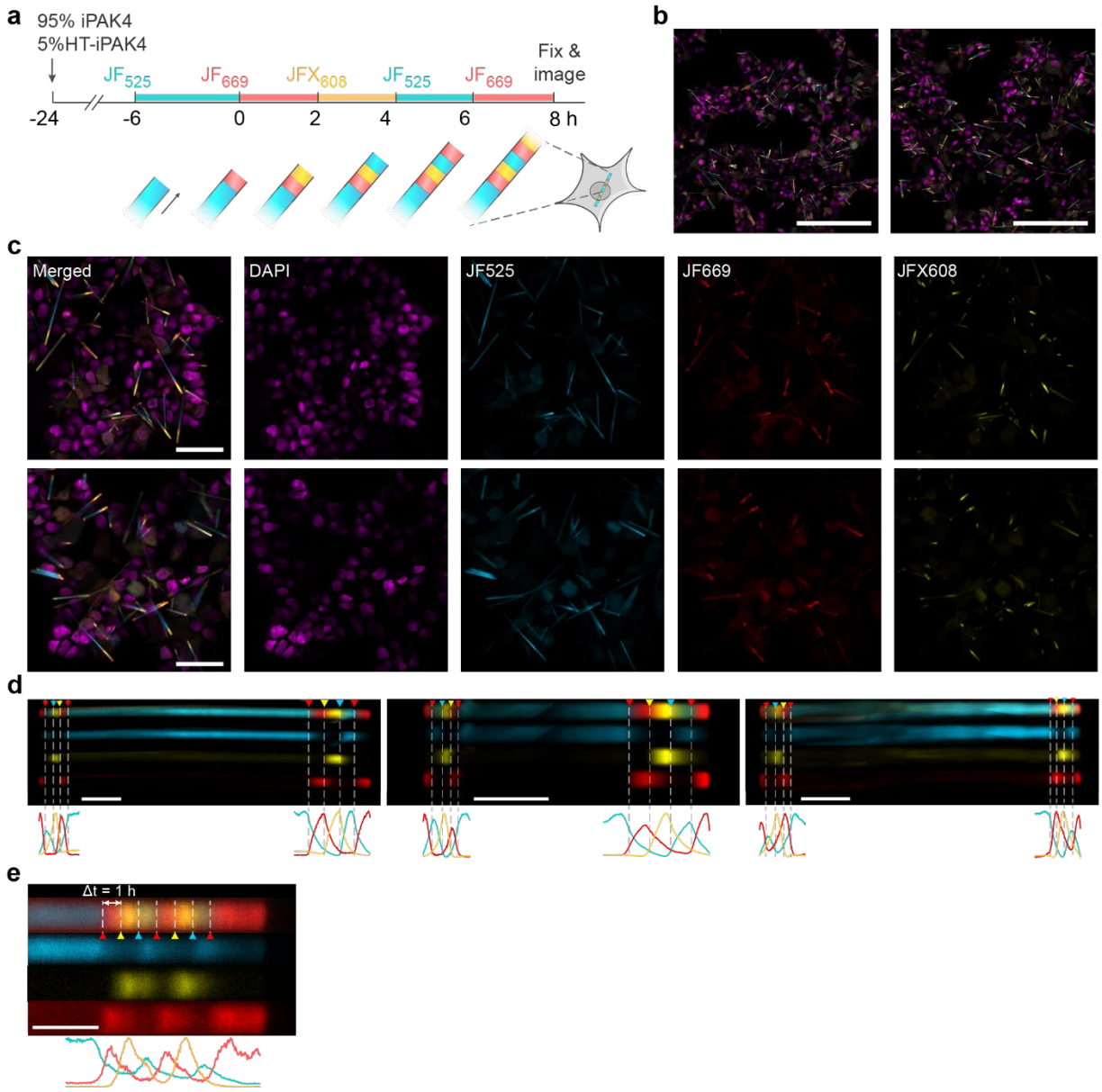


**Figure S7. Color stripes in sequentially labeled HT-iPAK4 fibers in HEK293T cells.** Related to Fig. 2. **a**, Scheme for multi-color labeling of intracellular iPAK4 fibers. HEK293T cells were co-transfected with CMV::iPAK4 (95%) and CMV::HT-iPAK4 (5%). After the onset of fiber growth, cells were washed at $\Delta t$ = 2 h intervals in the sequence $JF_{525}$, $JF_{669}$, $JFX_{608}$, $JF_{503}$, $JF_{669}$. **b.** Low-magnification images showing representative FOVs after the four dye switches. Scale bars: 200 μm. **c.** Magnified images showing the representative FOVs after the four dye switches. Scale bars: 50 μm. **d**. Images of single HT-iPAK4 fibers labeled with four dye transitions on each end. Scale bars 10 μm. **e,** Fiber end tagged with seven dye transitions at $\Delta t$ = 1 h. Scale bar 5 μm. (**d**,**e**) Each image panel shows a composite image of a fiber (top), the three-color channels individually (middle), and the line-profiles through each color channel (bottom). Blue: $JF_{525}$, Yellow: $JFX_{608}$, Red: $JF_{669}$.

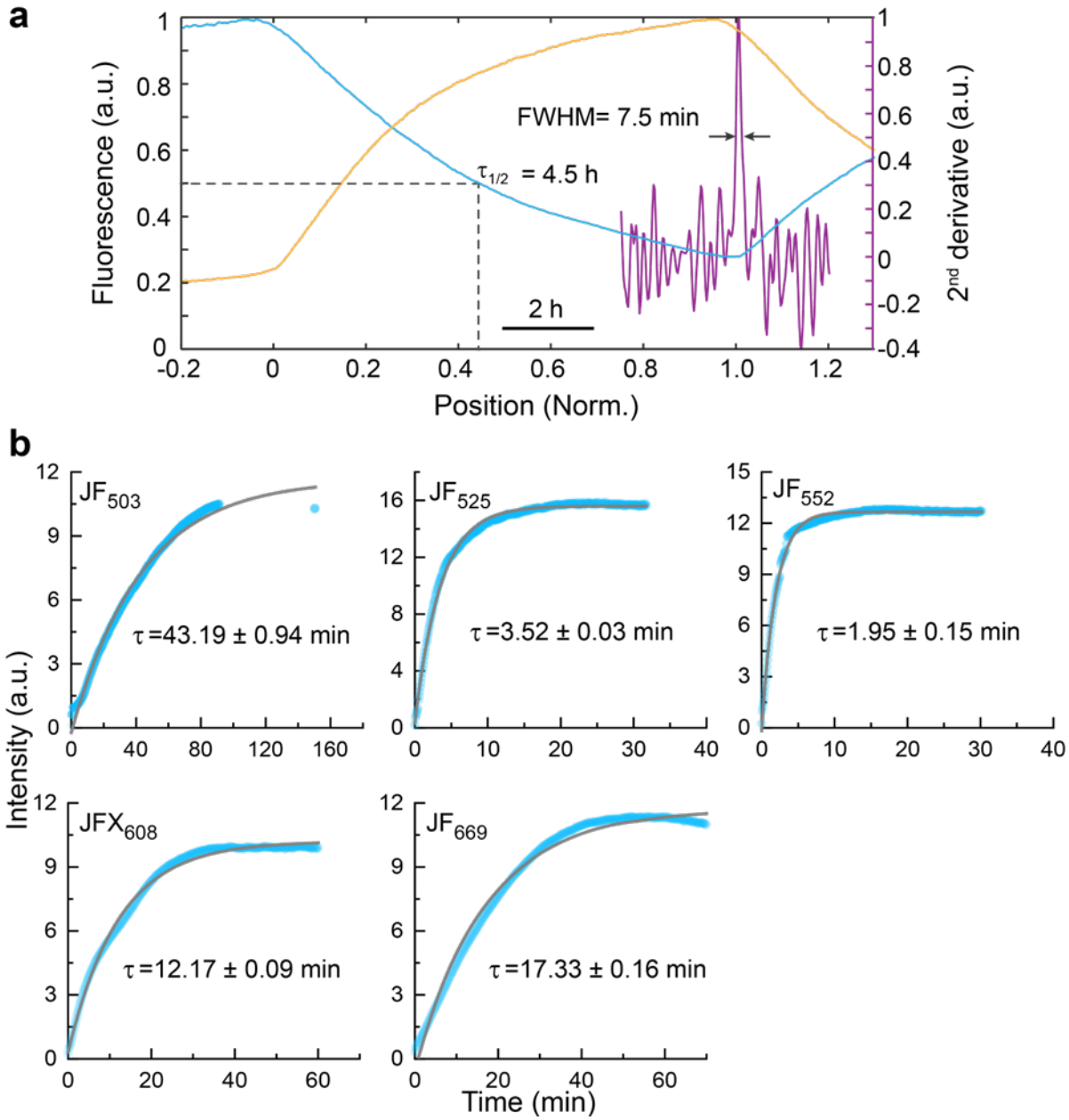


**Figure S8. Kinetics of HT dye labeling and turnover in HEK293T cells.** Related to Fig. 2. **a**, Mean fluorescence profile of fibers with dye switches $JF_{525}$ to $JF_{669}$ at $t$ = 0 and $JF_{669}$ to $JF_{525}$ at $t$ = 10 h (Blue: $JF_{525}$, yellow: $JF_{669}$, $N$ = 200 fibers, length normalized to 0 – 1). The half-life of soluble labeled HT-iPAK4 was 4.5 h, set by the rate of incorporation into the growing fiber. The sharpness of the dye transition was 7.5 min, as calculated by the width of the peak in the second derivative of fluorescence vs position (purple). **b**, Kinetics of HT dye reaction in HEK293T cells. HEK293T cells expressed a nucleus-targeted HT construct (HT-NLS, Addgene #82518) were incubated with 1 μM of the indicated dye and nuclear fluorescence was monitored as a function of time.

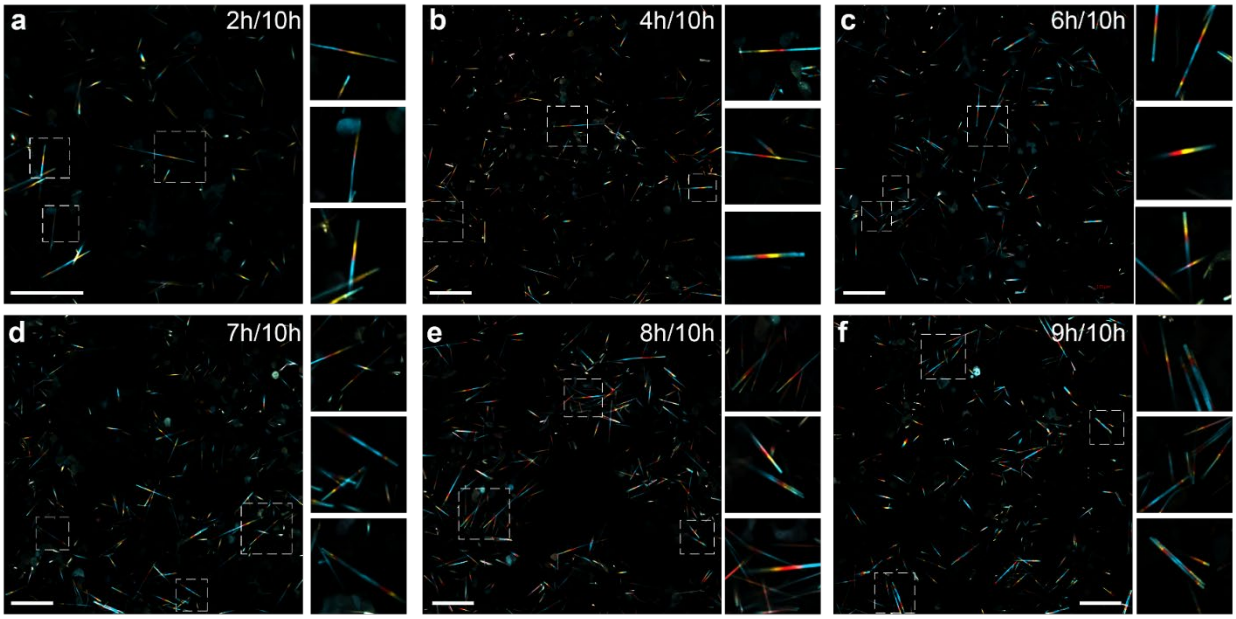


**Figure S9. Low-magnification images of HT-iPAK4 fibers with multiple fiducial timestamps.** Related to Fig. 3. Images show fibers initially labeled with $JF_{525}$, switched to $JF_{669}$ at $t$ = 0, $JFX_{608}$ at $t = X$, and back to $JF_{525}$ at $t$ = 10 h, for $X$ = 2, 4, 6, 7, 8, and 9 h. Insets show the regions in the dashed boxes. Scale bars 100 μm.

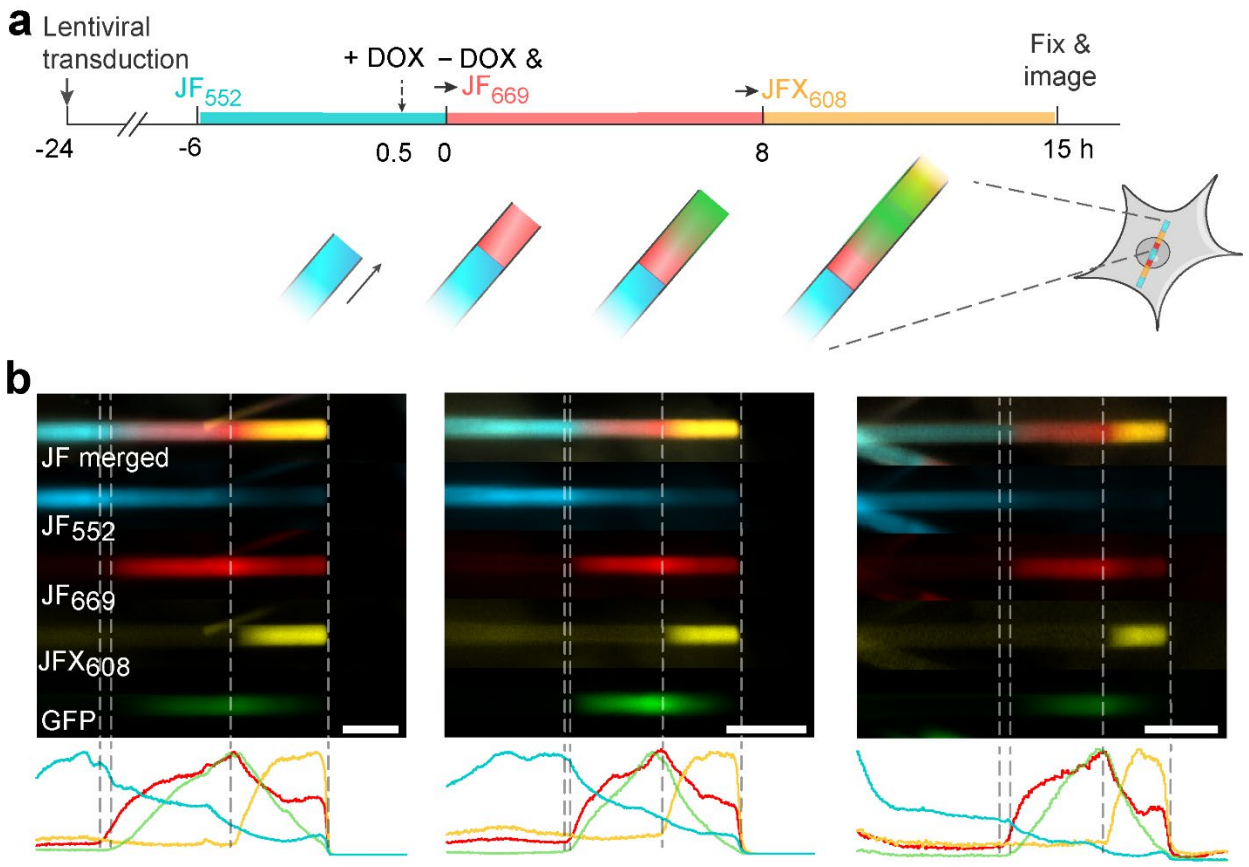


**Figure S10. Recordings of impulse response of protein expression following pulsed doxycycline (DOX) activation in HEK293T cells.** Related to Fig. 4. **a,** Experimental protocol for recording time-tagged response of eGFP-iPAK4 expression triggered by a brief pulse of DOX exposure. Transitions to $JF_{669}$ at t = 0 and to $JFX_{608}$ at t = 8 h provided fiducial timestamps. Transcription was activated via addition of 2 μg/mL DOX at t = -0.5 h, followed by a thorough wash at t = 0 h. **b,** Three representative examples showing the GFP intensity profiles on the protein ticker tapes. Top: representative images. Bottom: fluorescence line profiles. Scale bars: 10 μm.

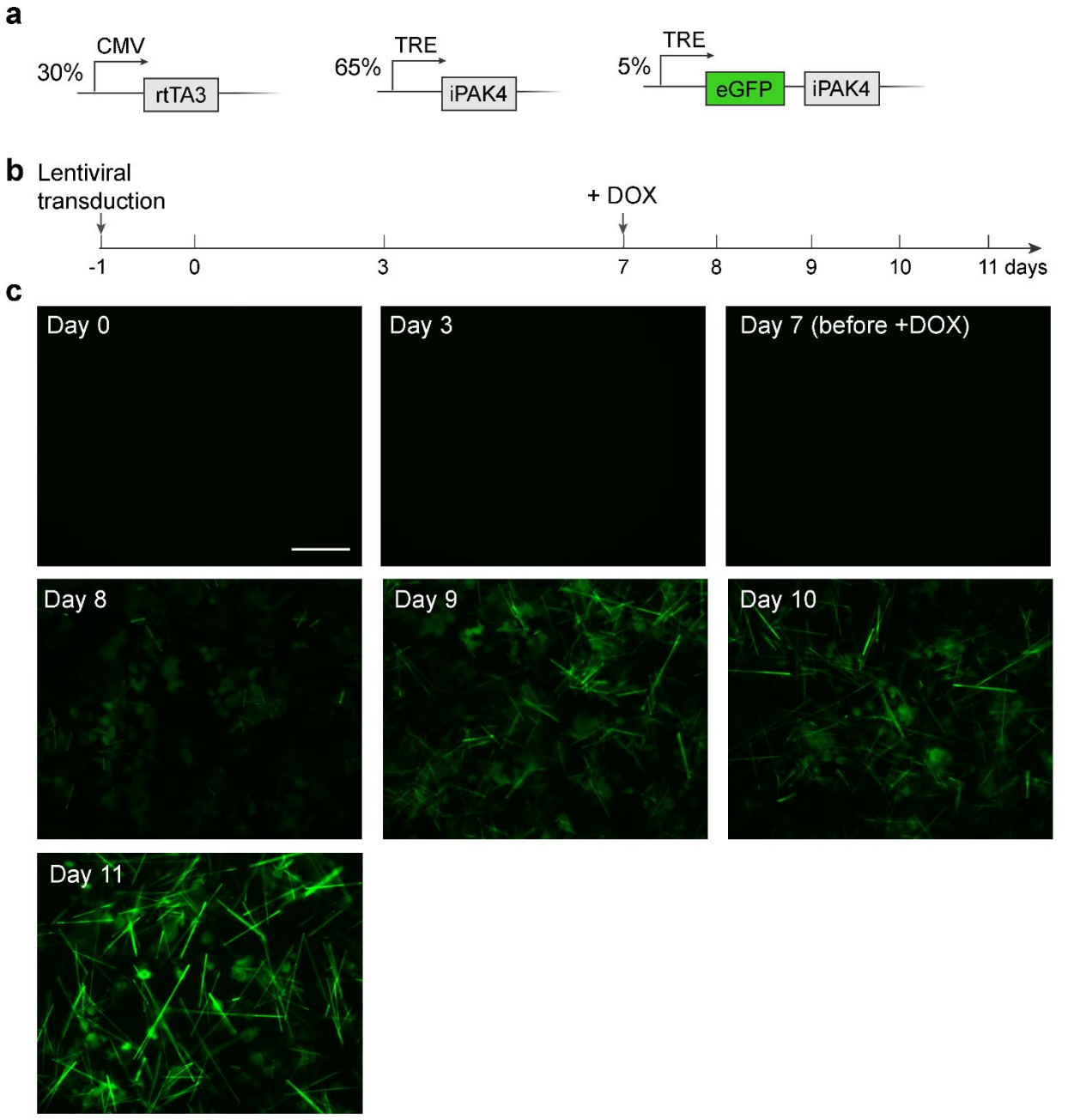


**Figure S11. Controlled onset of iPAK4 fiber growth with Tet-ON system in HEK293T cells.** Related to Fig. 4. **a,** Genetic constructs for Tet-ON control of the iPAK4 scaffold. **b**, Experimental protocol for controlling the onset of iPAK4 expression and fiber growth. DOX was added at day 7 after lentiviral transduction. **c,** Representative images taken at different days after lentiviral transduction. Scale bar 100 μm.

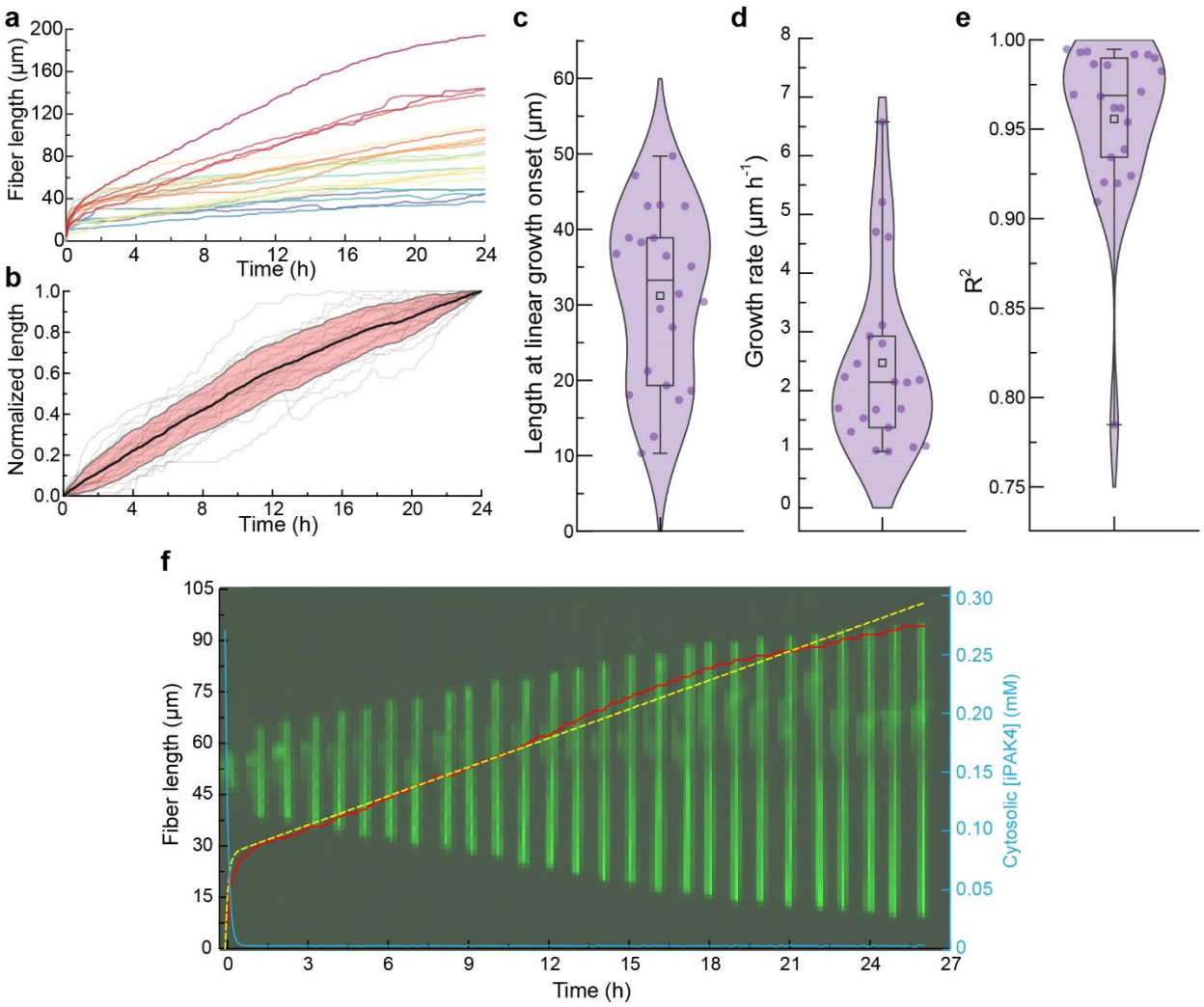


**Figure S12. iPAK4 fiber growth kinetics in primary neuron culture.** Related to Fig. 5. **a.** Growth profiles aligned by nucleation time (N = 22 fibers). **b,** Mean (black) and standard deviation (red fill) of growth profiles during the linear growth phase (N = 22 fibers, grey lines). **c-e**, Statistics of fiber growth, showing **c,** fiber length at the transition from initial nucleation to linear growth. **d**, Linear-phase growth rate. **e**, $R^2$ of the fit of the linear-phase growth to a straight line. In **c-e**, fibers were randomly selected from **Movie S4**. Box bounds: 25$^{th}$ and 75$^{th}$ percentile; whiskers: minimum and maximum; squares: mean; center lines: median. All data points are displayed, N = 22 fibers. **f.** Representative iPAK4 fiber growth profile in a cultured neuron (red solid line) and images at key frames (green). Simulated growth profile (yellow dashed line) and cytosolic iPAK4 concentration (blue solid line).

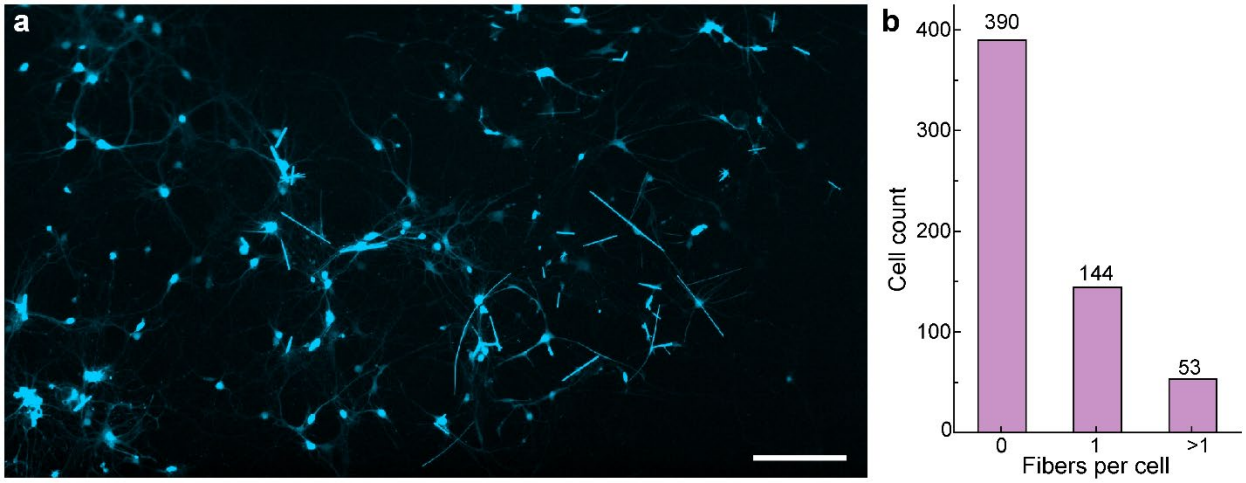


**Figure S13. Primary neuron culture with iPAK4 fibers.** Related to Fig. 5. **a,** Representative image of primary neuron culture with lentivirally delivered CMV::iPAK4 (95%) and CMV::HT-iPAK4 (5%) and stained with $JF_{552}$. Scale bar 200 µm. **b,** Distribution of the fiber count per cell in neurons. The fiber count was categorized into 0, 1 and >1 fibers per cell.

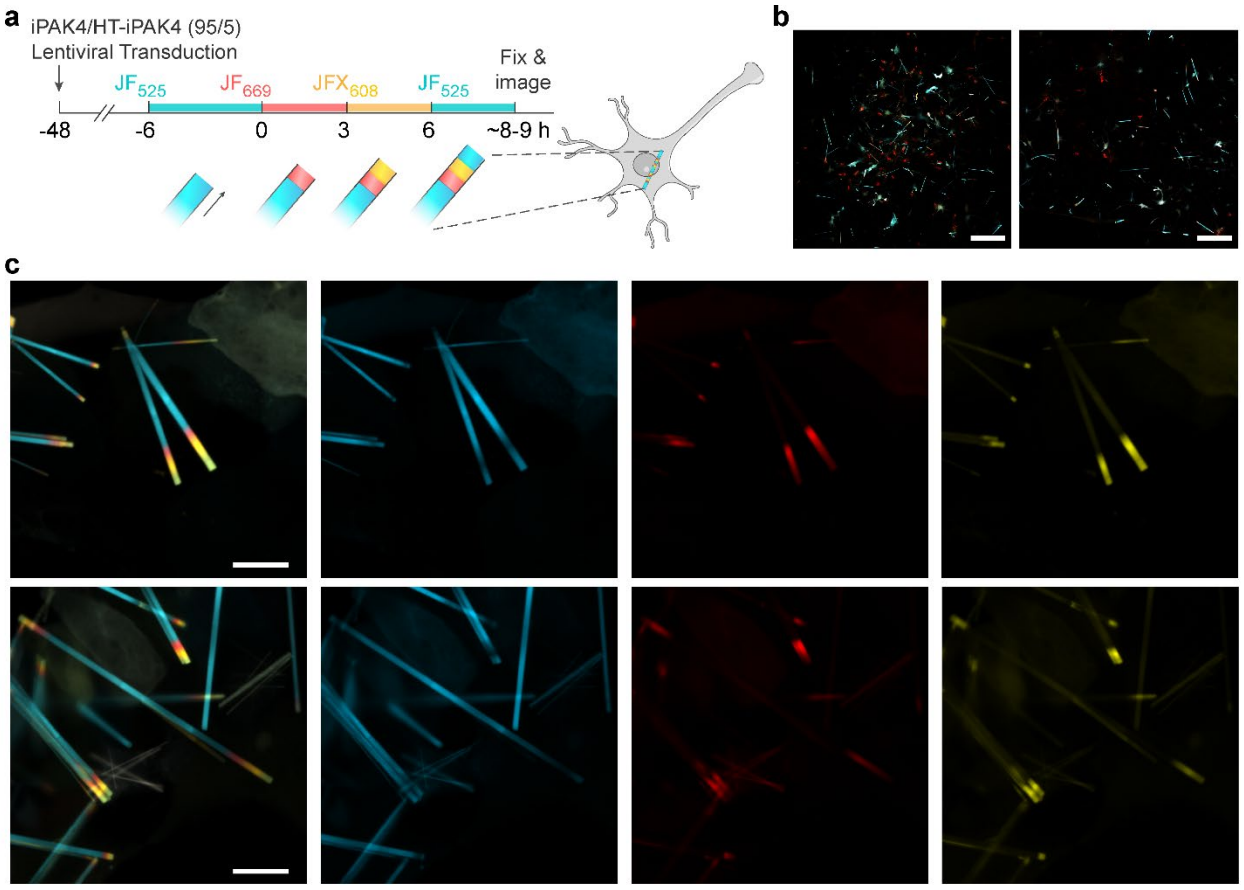


**Figure S14 Color stripes in sequentially labeled HT-iPAK4 fibers in primary neuron culture.** Related to Fig. 5. **a,** Scheme for multi-color labeling of intracellular iPAK4 fibers. In the experiment, HEK293T cells were co-infected with CMV::iPAK4 (95%) and CMV::HT-iPAK4 (5%). After the onset of fiber growth, cells were washed at $\Delta t$ = 3 h intervals in the sequence $JF_{525}$, $JF_{669}$, $JFX_{608}$, $JF_{525}$. **b.** Low-magnification images showing representative FOVs after the three dye switches. Scale bars: 100 μm. **c.** Magnified images showing the representative FOVs after the three dye switches. Scale bars: 20 μm.

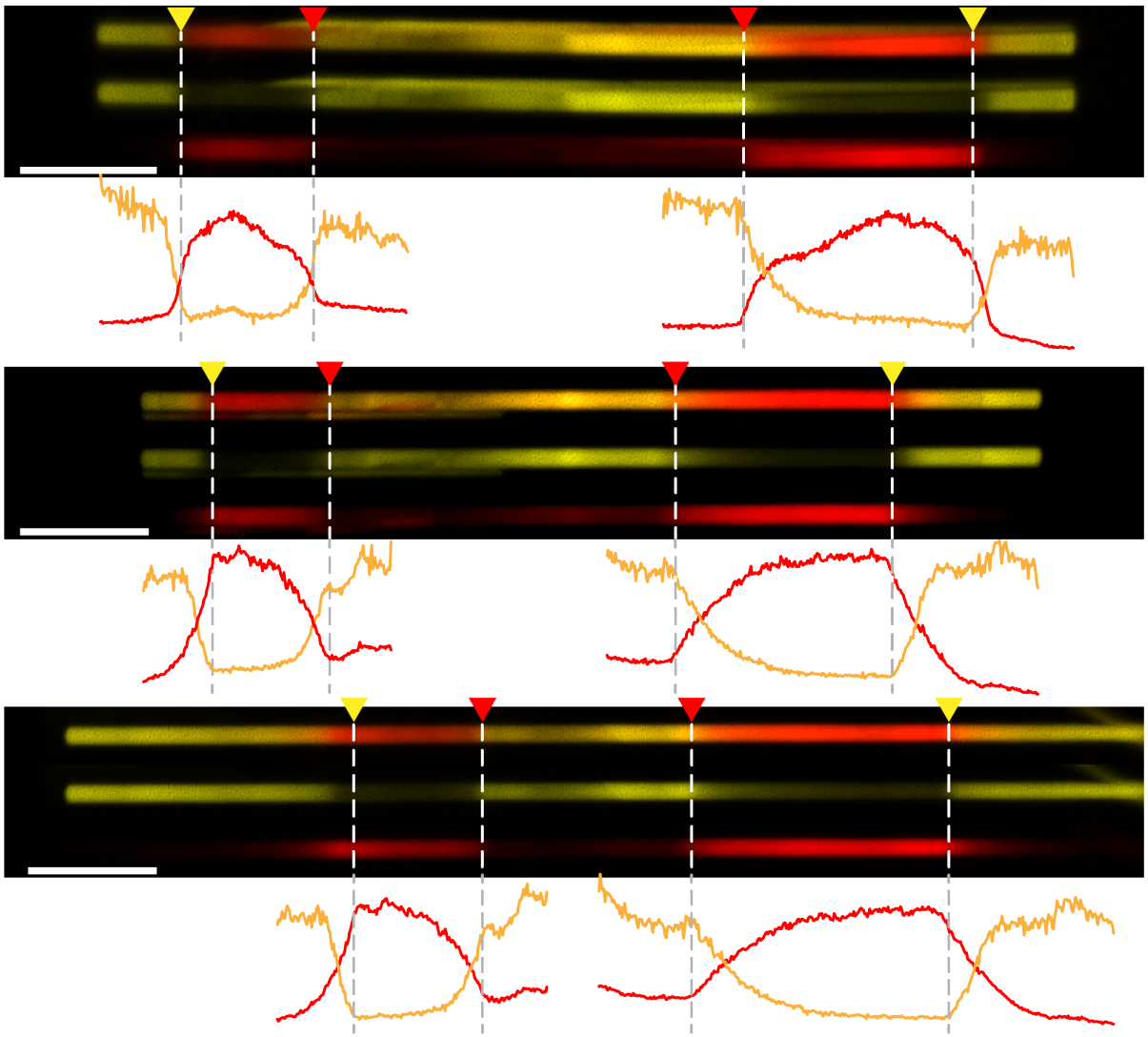

**Figure S15. Fiducial timestamps in neurons expressing HT-iPAK4.** Related to Fig. 5. Neurons were co-infected with lentivirus encoding CMV::iPAK4 (90%) and CMV::HT-iPAK4 (10%). Neurons were initially labeled with $JFX_{608}$ for 24 h, then with $JF_{669}$ for 24 h, and then with $JFX_{608}$ for another 24 h. Images show individual fibers (top), the $JFX_{608}$ (yellow) and JF669 (red) color channels separately (middle), and fluorescence profiles of each color channel (bottom). Scale bars 10 μm.

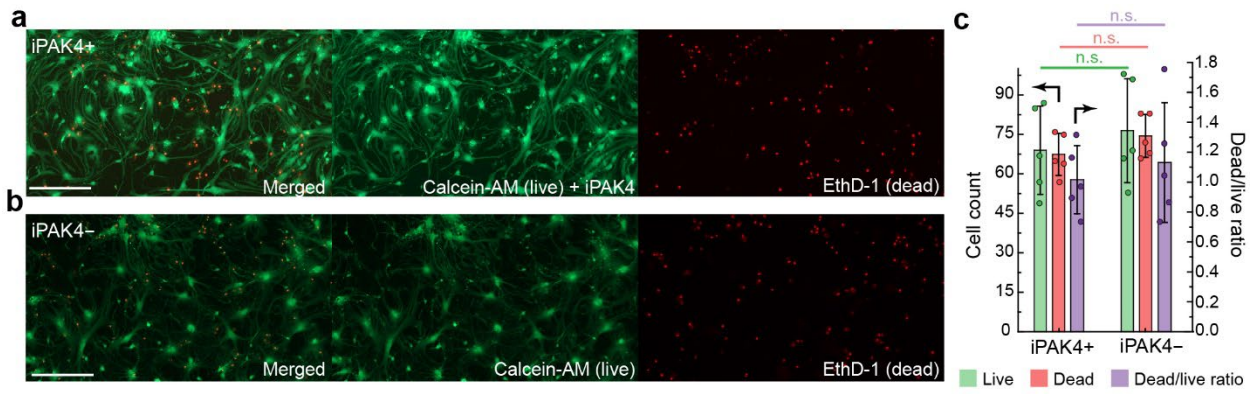


**Figure S16. iPAK4 fibers do not affect neuronal survival.** Related to Fig. 5. **a,** Primary neuron culture infected by CMV::iPAK4 (95%) and CMV::HT-iPAK4 (5%) lentiviruses with fiber formation in the cells. Scale bar: 200 µm. **b,** Neuron culture without any lentiviral infection. Green: Live cells (calcein-AM); Red: Dead cells (EthD-1). The assay was performed at day 6 after lentiviral infection. Many iPAK4 fibers are present in **a** (fibers share the green channel with calcein-AM). Scale bar: 200 µm. **c**. Statistical comparison of the live-cell and dead-cell populations, and dead/live cell ratio in iPAK4+ and iPAK4- groups (N = 5 fields of view per group). Error bars: mean ± SD.

nature research

Corresponding author(s): Adam E. Cohen
Dingchang Lin

Last updated by author(s): Sep 13, 2022

# Reporting Summary

Nature Research wishes to improve the reproducibility of the work that we publish. This form provides structure for consistency and transparency in reporting. For further information on Nature Research policies, see our Editorial Policies and the Editorial Policy Checklist.

## Statistics

For all statistical analyses, confirm that the following items are present in the figure legend, table legend, main text, or Methods section.

| n/a | Confirmed |
|---|---|
| ☐ | ☒ The exact sample size (*n*) for each experimental group/condition, given as a discrete number and unit of measurement |
| ☐ | ☒ A statement on whether measurements were taken from distinct samples or whether the same sample was measured repeatedly |
| ☐ | ☒ The statistical test(s) used AND whether they are one- or two-sided<br>*Only common tests should be described solely by name; describe more complex techniques in the Methods section.* |
| ☒ | ☐ A description of all covariates tested |
| ☒ | ☐ A description of any assumptions or corrections, such as tests of normality and adjustment for multiple comparisons |
| ☐ | ☒ A full description of the statistical parameters including central tendency (e.g. means) or other basic estimates (e.g. regression coefficient) AND variation (e.g. standard deviation) or associated estimates of uncertainty (e.g. confidence intervals) |
| ☐ | ☒ For null hypothesis testing, the test statistic (e.g. *F*, *t*, *r*) with confidence intervals, effect sizes, degrees of freedom and *P* value noted<br>*Give P values as exact values whenever suitable.* |
| ☒ | ☐ For Bayesian analysis, information on the choice of priors and Markov chain Monte Carlo settings |
| ☒ | ☐ For hierarchical and complex designs, identification of the appropriate level for tests and full reporting of outcomes |
| ☐ | ☒ Estimates of effect sizes (e.g. Cohen's *d*, Pearson's *r*), indicating how they were calculated |

*Our web collection on statistics for biologists contains articles on many of the points above.*

## Software and code

Policy information about availability of computer code

| | |
|---|---|
| Data collection | We used Zeiss LSM980, Elyra7, Discoverer7, or Olympus IX76 for data acquisition. The associated Zen Blue or Zen Black softwares (Zeiss) were used for data collection. |
| Data analysis | Linear spectral unmixing was performed using Zen Blue (Zeiss). Matlab 2020 and ImageJ 1.53k were used for other data analyses. The code involved custom scripts comprising standard image processing steps, written for the specifics of the datasets, without any novel algorithms. Details of data analyses can be found in the manuscripts. |

For manuscripts utilizing custom algorithms or software that are central to the research but not yet described in published literature, software must be made available to editors and reviewers. We strongly encourage code deposition in a community repository (e.g. GitHub). See the Nature Research guidelines for submitting code & software for further information.

## Data

Policy information about availability of data

All manuscripts must include a data availability statement. This statement should provide the following information, where applicable:

- Accession codes, unique identifiers, or web links for publicly available datasets
- A list of figures that have associated raw data
- A description of any restrictions on data availability

Data comprising images and time-lapse recordings of iPAK4 fibers, and patch clamp recordings, are available from the corresponding authors upon reasonable request.

# Field-specific reporting

Please select the one below that is the best fit for your research. If you are not sure, read the appropriate sections before making your selection.

☒ Life sciences ☐ Behavioural & social sciences ☐ Ecological, evolutionary & environmental sciences

For a reference copy of the document with all sections, see nature.com/documents/nr-reporting-summary-flat.pdf

# Life sciences study design

All studies must disclose on these points even when the disclosure is negative.

| | |
|---|---|
| Sample size | For each experiment, sample size was as large as could be practically achieved by our microscopic imaging, given the number of cells/fibers available in the images taken. Sample sizes were not pre-defined. Proper statistical analyses were performed to account for technical and biological variability. |
| Data exclusions | Protein fibers were excluded if the fiber was oriented out of the focal plane or if the fiber overlapped with another fiber, preventing acquisition of a clear image. All other fibers were included. |
| Replication | All experiments were performed over at least three rounds of cell culture and were reliably reproduced. |
| Randomization | Allocation of individual samples into control and experimental groups was done randomly. For each experiment a dish of cells was selected at random from the incubator, and a matched dish was selected at random for control conditions, where applicable. |
| Blinding | This is not applicable to our study, as the experiments needed to be performed at designated conditions and time points with known reagents. Analyses were performed in batch processing across experimental and control conditions using common parameters throughout. |

# Reporting for specific materials, systems and methods

We require information from authors about some types of materials, experimental systems and methods used in many studies. Here, indicate whether each material, system or method listed is relevant to your study. If you are not sure if a list item applies to your research, read the appropriate section before selecting a response.

## Materials & experimental systems

| n/a | Involved in the study |
|---|---|
| ☒ | ☐ Antibodies |
| ☐ | ☒ Eukaryotic cell lines |
| ☒ | ☐ Palaeontology and archaeology |
| ☐ | ☒ Animals and other organisms |
| ☒ | ☐ Human research participants |
| ☒ | ☐ Clinical data |
| ☒ | ☐ Dual use research of concern |

## Methods

| n/a | Involved in the study |
|---|---|
| ☒ | ☐ ChIP-seq |
| ☒ | ☐ Flow cytometry |
| ☒ | ☐ MRI-based neuroimaging |

## Eukaryotic cell lines

Policy information about cell lines

| | |
|---|---|
| Cell line source(s) | HEK293T cell line, purchased from ATCC, was used in this study. Primary hippocampal neurons were isolated from E18 rats (BrainBits) for culture. |
| Authentication | The cell line used in this study was purchased directly from ATCC so additional authentication was not performed. No other cell lines were concurrently cultured in our lab, so mixup was not possible. |
| Mycoplasma contamination | The cell line was tested negative for mycoplasma contamination. |
| Commonly misidentified lines (See ICLAC register) | No commonly misidentified cell lines were used. |

## Animals and other organisms

Policy information about studies involving animals; ARRIVE guidelines recommended for reporting animal research

| | |
|---|---|
| Laboratory animals | Neurons were dissociated from E18 rat pups of both sexes. Dissections were performed at Brainbits llc. |
| Wild animals | *Provide details on animals observed in or captured in the field; report species, sex and age where possible. Describe how animals were* |

| | |
|---|---|
| Wild animals | *caught and transported and what happened to captive animals after the study (if killed, explain why and describe method; if released, say where and when) OR state that the study did not involve wild animals.* |
| Field-collected samples | *For laboratory work with field-collected samples, describe all relevant parameters such as housing, maintenance, temperature, photoperiod and end-of-experiment protocol OR state that the study did not involve samples collected from the field.* |
| Ethics oversight | Extracted tissue was commercially sourced (Brainbits llc) so IACUC approval was not required. |

Note that full information on the approval of the study protocol must also be provided in the manuscript.